Challenge Journal of
CONCRETE RESEARCH LETTERS

Vol.9 No.2 (2018)

acidic environment acoustic emission compressive strength concrete corrosion cracking deformation characteristics ductility durability energy absorption ferrocement fly ash mechanical properties palm oil fuel ash reinforced concrete self-compacting concrete serviceability load silica fume steel mesh strength strengthening water a[illegible]ion

ISSN 2548-0928

TULPAR ACADEMIC PUBLISHING

Challenge Journal of Concrete Research Letters

E-mail: *cjcrl@challengejournal.com*

Web page: *cjcrl.challengejournal.com*

TULPAR Academic Publishing
www.tulparpublishing.com

Challenge Journal of Concrete Research Letters

CONTENTS

Research Articles

Experimental and numerical study of the behavior of RC slabs with openings reinforced by metal mesh under impact loading **37-51**

Yousry B. I. Shaheen, Ghada Mousa Hekal, Ahmed Khaled Fadel

Prediction of self compacted rubberized concrete properties using Taguch methods **52-61**

Mohamed Safaan, Fatma M. Eid, Amal A. Nasser, Mohamed Emara

Reviews

Reinforcement corrosion in coastal and marine concrete: A review **62-70**

Saha Dauji

Challenge Journal of Concrete Research Letters

Research Article

Experimental and numerical study of the behavior of RC slabs with openings reinforced by metal mesh under impact loading

Yousry B. I. Shaheen, Ghada Mousa Hekal *, Ahmed Khaled Fadel

Department of Civil Engineering, Menoufia University, Shebin ElKoum, Menofia, Egypt

ABSTRACT

The main objective of the following work is to inspect the effect of reinforcing metal mesh on the behavior of slabs with openings under impact loadings. Based on an earlier numerical study by Shaheen et al. (2017), slabs with mid-side openings revealed the worst behavior regarding to deflection and cracked pattern when subjected to impact loading compared to other slabs with different locations of openings. Hence, the present work focuses specifically on this type of slabs and the variation in their behavior when reinforced by welded or expanded metal mesh. Seven specimens were prepared and tested in Faculty of Engineering, Menoufia University, Egypt. Moreover, a FE model for the slabs was built using Abaqus 6.14 and verified against test results. It was found that expanded metal mesh had a significant effect on reducing deflection due to impact load as well as controlling of cracks in contrast with welded metal mesh.

ARTICLE INFO

Article history:
Received 10 May 2018
Accepted 29 May 2018

Keywords:
RC plates
Openings
Experimental
Impact
Reinforcing metal mesh
Abaqus

1. Introduction

Structures, during their life time may be vulnerable to different kinds of hazards. In comparison with other threats, impact loads are distinguished by the intensity of the localized pressures that act on different building components making it several orders of magnitude greater than other hazards. Recently, considerable work has been carried out in an effort to develop impact-resistant design techniques and to advance the performance of different reinforced concrete elements subjected to impact loads. For example, Attallah (2012) investigated nonlinear behavior of fixed-ended RC columns subjected to impact loads using Abaqus software. Ahmed (2014) explored the dynamic behavior of beam under impact load using Abaqus program. The selected beam was previously tested under subjected to free-falling steel hammer by Kishi (2004). The studied parameters included damping, tension and compression stiffness recovery, damage parameter-strain/displacement relations and friction coefficient to choose the best performing FE analysis model. Thilakarathna et al. (2009) also investigated behavior of axially loaded concrete columns subjected to transverse impact loads.

In contrast with other structural elements, slabs are slender elements which are often exposed to flexural, shear or both modes of failure if subjected to impact loads. The effects of extreme load conditions on RC structures have been studied by many researchers to develop safe and efficient design procedures. For example, Batarlar (2013) presented the findings of an experimental program designed for investigating the behavior of RC slabs under low-velocity impact loads. The program included a comparison between static and dynamic behavior of three pairs of simply supported slabs. The results obtained from these tests revealed that the impact behavior of slabs differs significantly compared to their static behavior. Tahmasebinia (2008) presented experimental and numerical modelling of reinforced concrete slabs subjected to impact loading using Abaqus software. This study discussed the effect of using lacing and vertical shear reinforcement in behavior of slabs. The FE models based on simulating impact behavior of different types of concrete models were investigated. In the study, concrete was modelled in Abaqus using both Drucker-Prager and Concrete Damage Plasticity models. Andersson (2014) investigated the static and the dynamic load capacity of steel fiber reinforced shotcrete (SFRC) by

* *Corresponding author*. Tel.: +20-106-985-6009 ; E-mail address: gahda.mousa@sh-eng.menofia.edu.eg (G. M. Hekal)
ISSN: 2548-0928 / DOI: https://doi.org/10.20528/cjcrl.2018.02.001

experimental tests and numerical simulation in order to predict the capacity of the inner lining system. It was found that the simulation of impact loads on slabs showed good agreement in both peak load and peak vertical displacement, but simulations of the inner lining system showed significantly larger load capacity than the concrete slabs. Finally, the generated FE-model was also able to predict the failure mode and crack widths with a fair accuracy. Ali and Al-Khafaji (2015) presented a theoretical study of the nonlinear behavior of reinforced concrete slabs subjected to impact loads using ANSYS software. The study included the effects of reinforcement ratio, dimensions of slabs and support conditions. It was found that the central deflections of the slabs under impact became smaller as the tensile reinforcing steel ratio increases, but the rate of the decreases in the deflection is less for high steel reinforcement ratio. Also, those deflections were found to be oscillatory in nature but not in-phase with the applied load. However, clamping edges of the slabs resulted in larger oscillation frequencies as compared to the case of simple supports. Sudarsana et al. (2015) presented the results of experimental program for the impact behavior of high performance concrete slabs in comparison with reinforced cement concrete slabs as control specimens. The results showed that the HPC slabs possess higher number of blows for first crack and ultimate failure, higher impact load and energy absorption. Elavenil and Knight (2012) investigated the dynamic behavior of steel fiber reinforced concrete slabs under impact loading with respect to displacement, velocity and acceleration. It was found that when the aspect ratio of fibers is 50 and 75 there is a marginal increase in energy absorption for change in fiber content from 0.5 to 0.75%. There is a steep increase in energy absorption for a steel fiber content of 1% when the aspect ratio of fiber is 100. Tahmasebinia and Remennikov (2008) examined several types of RC slabs numerically and compared with experimental observations. Shear reinforcement was considered during testing and analysis. Shaheen and Abusafa (2017) investigated the possibility of using ferrocement concrete to rehabilitee the damaged plates which failed under impact load. The study presented the comparison between the results of the first crack loads, the ultimate loads and the deflections in the cases of repeated impact loads and static loads. The obtained results reached emphasized good deformation characteristics, high first crack and ultimate load, high ductility, energy absorption properties, and cracking pattern without spilling of concrete cover that is predominant.

More experimental tests and numerical investigations either on impact effects on RC slabs or enhancing dynamic behavior of RC slabs under impact were published by Saatci and Vecchio (2009), Mokhatar and Abdulla (2012), Yoo et al. (2012) and, Antunes and Masuero (2016).

Although slabs usually contain openings, the behavior of that type under impact loads is not completely addressed in literature. However, slabs with openings were studied in several research under different load conditions. For example, Boon et al. (2009) conducted an experimental work to determine the structural performance of one-way reinforced concrete (RC) slabs with rectangular opening under four points bending tests. The experiments showed that the presence of openings reduced the capacity of the slabs compared to slabs without openings.

Khajehdehi and Panahshahi (2014) conducted a sensitivity analysis where the effects of opening size (0, 6.25%, 14%, and 25% of the floor panel area) and out-of-plane loading (zero and full-service load) on the in-plane load deformation characteristic of the floor panels were investigated. The results indicated that the drop in ultimate in-plane load capacity of the floor diaphragm due to presence of out-of-plane service loading became less significant as the opening size increased (4% for 25% opening vs. 15% for the solid slab). Also, the first significant variation from the initial linear portion of the in-plane load-deformation curve moved up from 30% to about 50% of the ultimate load capacity for the slab with larger size openings.

Selime et al. (2011) reported field tests on the use of carbon fiber-reinforced polymer (CFRP) composite strengthening techniques to restore the flexural capacity of RC slabs after having openings cut out in the positive moment region. The uniqueness of that study is that the tests were performed on an existing multistory RC building that was scheduled for demolition. Five tests on five different slabs were conducted using three different strengthening techniques—namely, externally bonded (EB) CFRP plates, EB CFRP plates with CFRP anchors, and near-surface mounted (NSM) CFRP strips—to determine the most effective system for strengthening. Test results showed that the three strengthening techniques increased the load-carrying capacity of the slabs with openings, with the NSM technique being more effective than the EB technique. However, the use of CFRP anchors to mechanically anchor the EB plates prevented complete detachment, and hence enabled the restoration of the slab to its full flexural capacity.

Shaheen et al. (2017) investigated the dynamic behavior of slabs with openings under impact; a series of finite element models with different positions, numbers and shapes of openings were built and analyzed using Abaqus software. The studied parameters included mid-point deflection, maximum deflection along opening perimeter, tension damage and cracked zones. It was concluded that the worst behavior regarding to deflections and damaged area appeared when the openings were in mid-side of slabs.

The current research presents an experimental and numerical investigation of RC slabs with circular and square openings in their mid-side. Welded and expanded metal meshes were added to some specimens to inspect their influence in improving impact load resistance of the tested slabs.

2. Specifications of the Tested Specimens

Seven specimens, one control and six with openings were prepared and cast in the Laboratory of Resistance and Testing of Materials at the Faculty of Engineering, Menoufia University. All test specimens have the same

dimensions of 1100×1100×30 mm. 10 mm clear cover was provided for the reinforcement from all sides and 6 mm clear cover was provided from the bottom face of the specimens (see Fig. 1). Specimens were reinforced by 1ø6 mm steel bars @ 150 mm arranged in mesh form. Two additional perpendicular bars were added under impact point on all samples to prevent penetration of projectile during test. Tested specimens labels, opening shape, opening dimensions, and reinforcement used are given in Table 1. To enhance the behavior of slabs, expanded and welded metal mesh were added to four specimens (see Fig. 2).

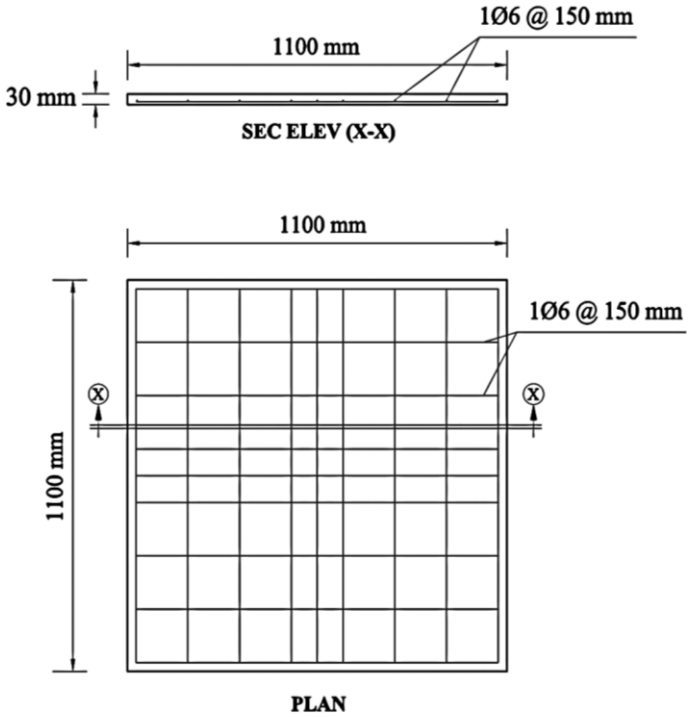

(a) Control specimen

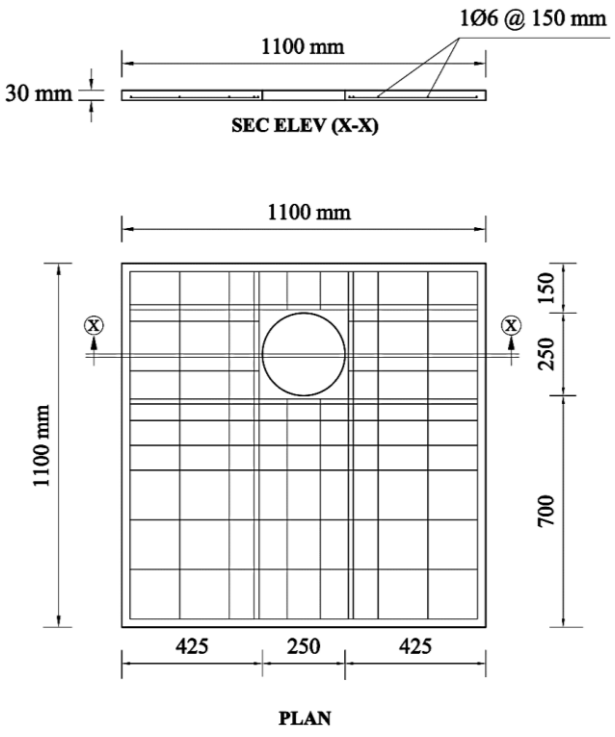

(b) Circular Opening specimen

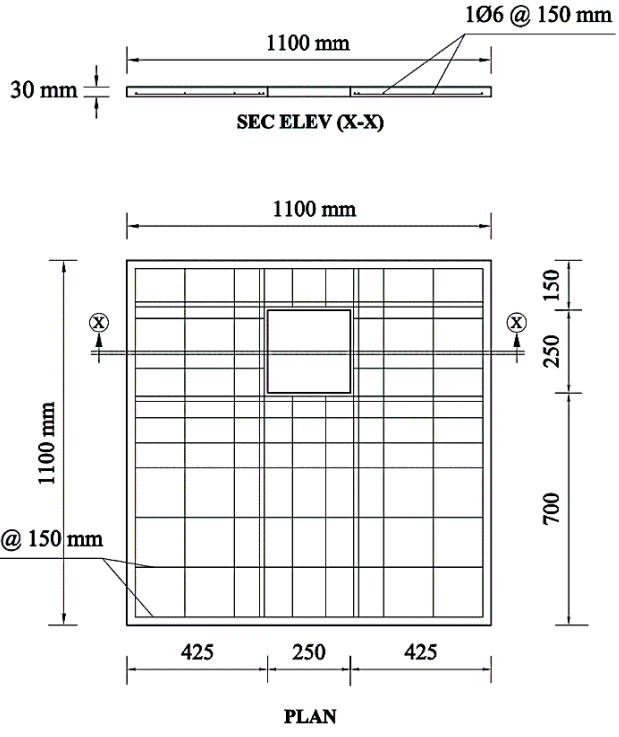

(c) Square Opening specimen

Fig. 1. Dimensions of tested specimens.

(a) S1

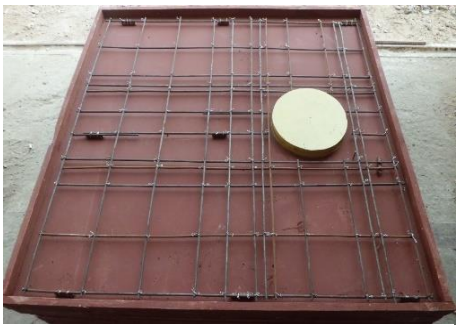

(b) S2

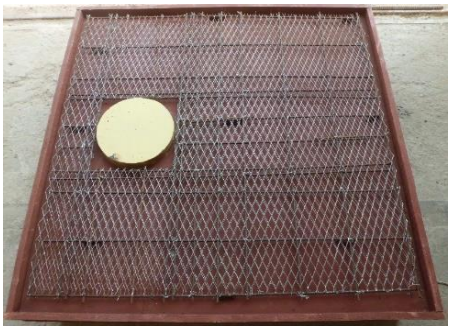

(c) S3

(d) S4

(e) S5

(f) S6

(g) S7

Fig. 2. Reinforcement of tested specimens.

Table 1. Specimen properties.

No.	Label	Opening		Steel Bars Reinforcement	Mesh Reinforcing	End Conditions
		Shape	Dimensions			
1	S1	-------	-------	1ø6 @ 150 mm	-------	Simply Supported
2	S2	Circular	Diameter = 250 mm		-------	
3	S3				Expanded	
4	S4				Welded	
5	S5	Square	250 x 250 mm		-------	
6	S6				Expanded	
7	S7				Welded	

3. Material Specifications

3.1. Concrete

The concrete mix used for manufacturing specimens was designed to be easy to operate and to have the ability to fill the small thickness of specimens without nesting. To control the width of cracks resulting from impact, polypropylene fiber was added to concrete mix. Table 2 shows the constituents of one-meter cube used in making the concrete mix.

Both compression and tensile strengths of the concrete mix were determined experimentally following Egyptian Standard Specifications, ES1658-4/2008, and ISO1920-3/2004. To determine compressive strength of concrete mix, cubic specimens with dimensions (150 × 150 × 150 mm) were cast and tested under compression at the ages of 7 days and 28 days after the day of casting as shown in Table 3. Three specimens were tested at each date. The tensile strength of the used concrete was determined by conducting Brazilian tensile test or indirect tensile test (see Fig. 3) on a cylindrical sample of diameter 150 mm and height 300 mm to be the standard tensile strength value equal to 85% of the tensile strength value of the Brazilian tensile test (according to Egyptian code of practice – Appendix 3 - Manual of laboratory tests of concrete materials) (F_t=2.45 MPa).

Table 2. Concrete mix quantities.

Constituent	Basalt	Sand	Cement	Meta Kaolin	Water	Super Plasticizer	Polypropylene fibers
Quantity (kg/m³)	1200	600	425	75	175	10	1.5

Table 3. Compression test results.

Period (days)		7days	28 days
		Peak compressive strength (MPa)	Peak compressive strength (MPa)
Cubic specimen no.	1	27.3	28.9
	2	`24.9	31.1
	3	25.6	33.2

3.2. Steel bars

Steel bars used for reinforcing were made of mild steel of cross sectional area 28.27 mm². The yield stress and ultimate stress of steel used were 280 and 380 MPa respectively.

3.3. Reinforcing steel mesh

Two types of reinforcing steel meshes were used in the test; welded and expanded as shown in Fig. 4. The technical specifications and mechanical properties of both types as provided by producing companies are given in Tables 4 and 5.

Fig. 3. Sample of Brazilian tensile test.

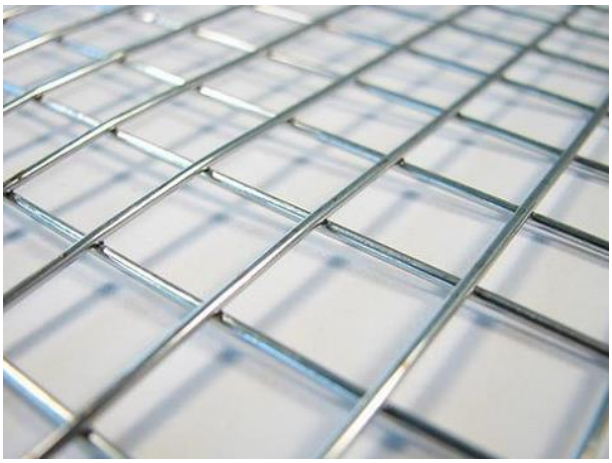

(a) Welded metal mesh

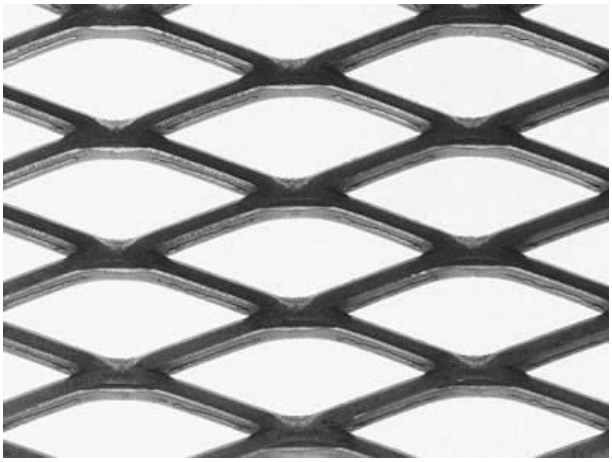

(b) Expanded metal mesh

Fig. 4. Reinforcing metal mesh.

Table 4. Technical specifications and mechanical properties of Welded Metal mesh.

Dimensions	15 mm × 15 mm
Cross Section Dimension	Diameter = 0.8 mm
Weight	440 gm/m^2
Modulus of Elasticity	170 GPa
Proof Stress	400 MPa
Ultimate Strength	600 MPa
Ultimate Strain × 10^{-3}	58.8
Proof Strain × 10^{-3}	1.17

Table 5. Technical specifications and mechanical properties of Expanded Metal mesh.

Diamond Size	20 mm × 45 mm
Cross Section Dimension (strand)	1.25 × 1.7 mm
Weight	1.35 kg/m^2
Sheet Size	1 m × 10 m
Modulus of Elasticity	125 GPa
Proof Stress	250 MPa
Ultimate Strength	350 MPa
Ultimate Strain × 10^{-3}	59.2
Proof Strain × 10^{-3}	9.7

4. Test Setup and Equipment

A steel frame was specifically designed and manufactured to support the tested specimens and to provide the simply supported end conditions. Frame was fabricated from steel channels (U.P.N) sections No 80, 100. Channels were arranged horizontally and vertically to provide frame with an adequate stiffness in all directions and to support impact load without significant deformations. To give simply supported end condition, steel bars of diameter 22 mm were welded along the perimeter of frame edges. Supported span of tested slabs in both directions was 950 mm which expresses the distance between every two opposite bars (see Fig. 5).

Seven impact tests were conducted with special attention being paid to maximum mid-point deflection and failure pattern of tension surface as two of the most important impact parameters. The steel frame was placed in an appropriate position that features with leveling of its surface. To ensure that, a babble level balance was used to adjust if the four sides were horizontal. A PVC pipe, with 160 mm diameter and 4.97 m, was installed vertically by connecting it from its mid-height to the steel frame using four steel angles. Besides, it was connected from upper lens to a ladder. Finally, its verticality was adjusted using the water balance (see Fig. 6). The next step was placing the specimen on the steel frame. At that time, the graduated ruler was placed below the specimen in a well seen position and near a steel indicator that was previously attached to the specimen during casting process to allow recording of displacement readings as shown in Fig. 7. Afterwards, a high frame rate camera was prepared to start recording by placing it in a suitable position near system and shedding it towards a graduated ruler.

(a) Before painting with anti-rust (b) After painting with anti-rust

Fig. 5. Supporting frame.

(a) Fixing pipe to frame (b) Fixing pipe to ladder (c) Adjusting verticality

Fig. 6. Installing PVC pipe.

A steel ball, with a weight of 13.7 Kg and 150 mm diameter, was dropped from a height of 4.97 m through the PVC pipe to fall directly on the test specimen. Fig. 8 displays complete test setup.

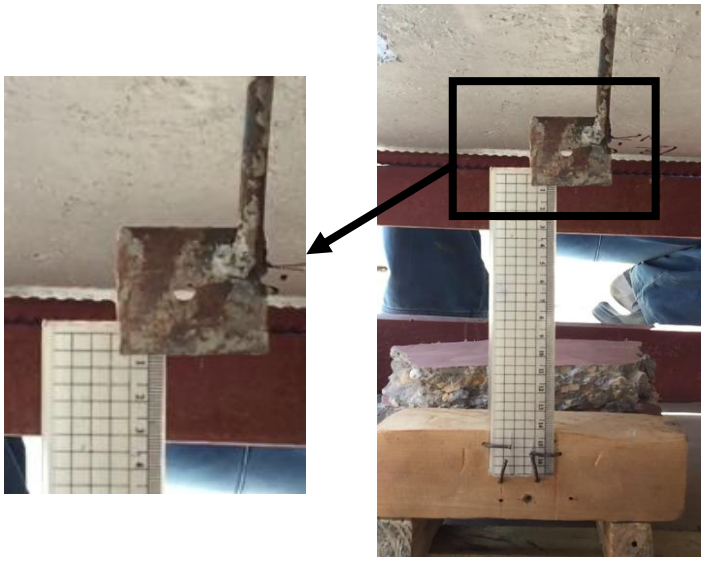

Fig. 7. Placing graduated ruler near steel indicator.

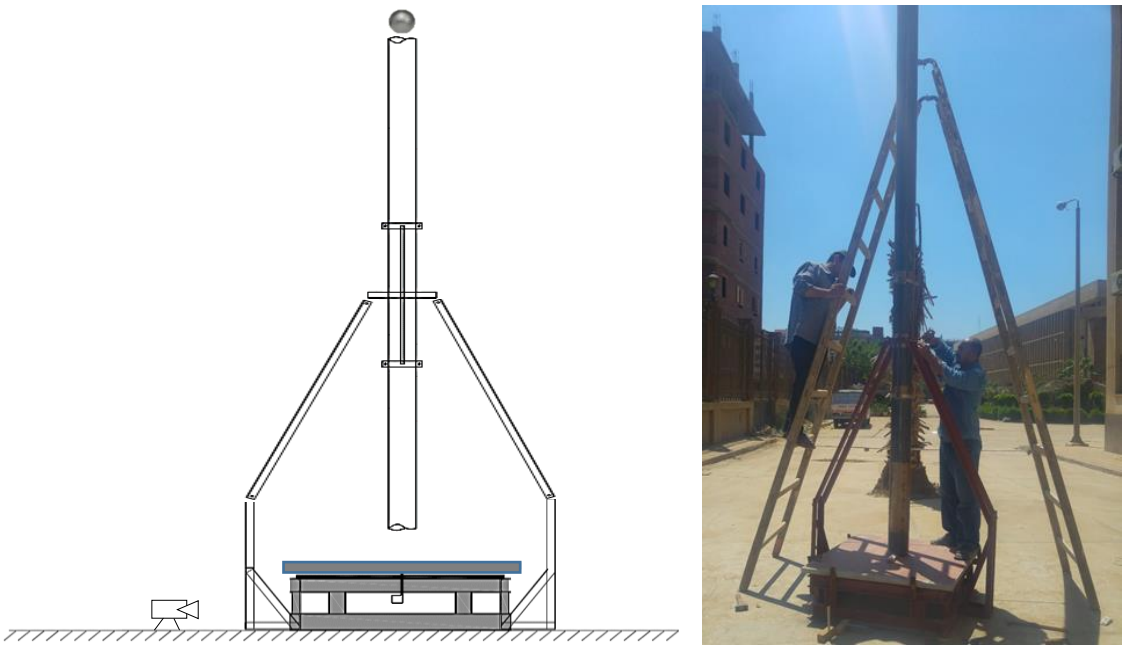

Fig. 8. Complete test setup.

5. Finite Element Model

The slabs of study were modelled as 3D structures in Abaqus. Concrete parts were modelled using C3D8R. The models were divided into fine elements with different sizes to allow quick analysis with sufficient accuracy. Total number of elements reached 32272 with sides varied from (25 × 10 × 5) mm to (10 × 10 × 5) mm. The fine element size was concentrated under impact region in the middle of slab as shown in Fig. 9 while the coarse size was provided near slab edges.

Steel bars and metal mesh were modelled using T3D2 elements that were embedded in the surrounding solid elements. Fig. 10 shows the modeling of welded and expanded metal mesh in Abaqus. Concrete material was modelled using Abaqus concrete damage plasticity model. This model uses the concept of isotropic damage elasticity in combination with isotropic compression and tensile plasticity to model the inelastic behavior of concrete. Tables 6 and 7 present concrete elastic properties and concrete damaged plasticity model parameter used in analysis. Steel reinforcement has approximately linear elastic behavior when the steel stiffness introduced by the Young's or elastic modulus keeps constant at low strain magnitudes. At higher strain magnitudes, it begins to have nonlinear, inelastic behavior, which is referred to as plasticity. The plastic behavior of steel is described by its yield point and its post-yield hardening. The shift from elastic to plastic behavior occurs at a yield point on a material stress-strain curve. The deformation of the steel prior to reaching the yield point creates only elastic strains, which is fully recovered if the applied load is removed. However, once the stress in the steel exceeds the yield stress, permanent (plastic) deformation begins to occur. Both elastic and plastic strains accumulate as the metal deforms in the post-yielding region. The stiffness of the steel decreases once the material yields. The plastic deformation of the steel material increases its yield stress for subsequent loadings. Table 8 shows the elastic properties of steel bars.

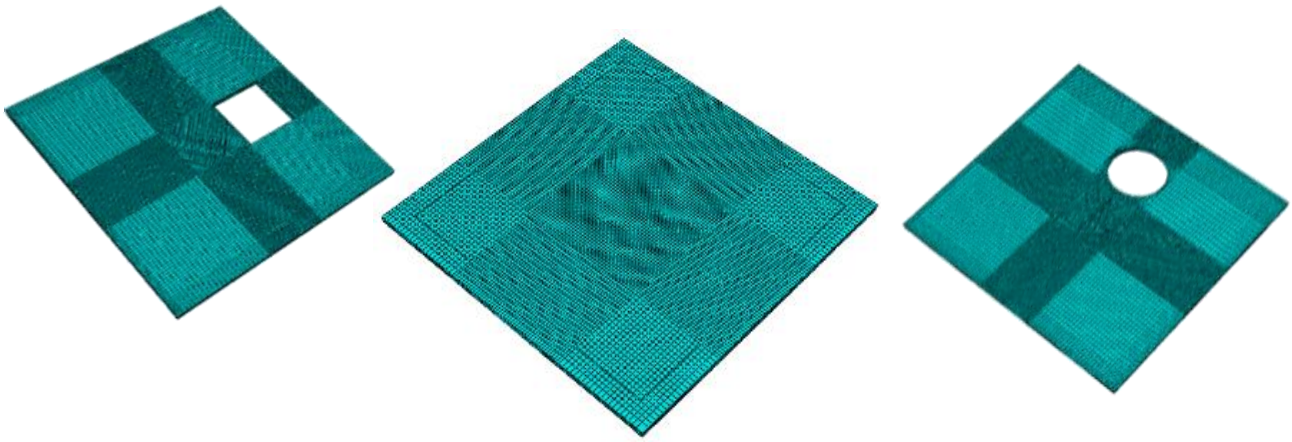

Fig. 9. Mesh description of concrete slabs models.

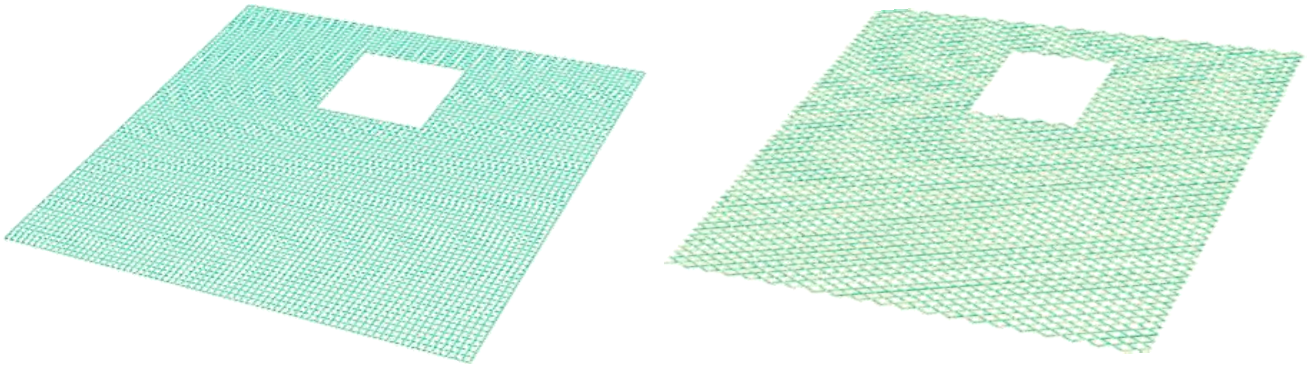

(a) Welded mesh (b) Expanded mesh

Fig. 10. Modeling of reinforcing metal mesh.

Table 6. Elastic properties of concrete.

Parameter	Value
Density	2.4×10^{-9} N/mm^3
Modulus of elasticity (Es)	21900 MPa
Poisson's ratio (υ)	0.168

Table 7. Concrete damaged plasticity parameters.

Parameter	Value
Dilation angle	42°
Eccentricity	0.11
fb0/fc0	1.35
K	0.68
Viscosity parameter	0.0001
Yield stress in compression	17 MPa
Cross bonding inelastic strain	0.0
Compressive ultimate stress	33MPa
Cross bonding inelastic strain	0.00158
Tensile failure stress	3.45 MPa

Table 8. Material properties of steel reinforcement.

Parameter	Value
Density	7.859×10^{-9} N/mm^3
Modulus of elasticity (Es)	199980 MPa
Poisson's ratio (υ)	0.3
Yield strength	250 MPa
Ultimate strength	360 MPa

The geometry of the steel ball was defined in all models using rigid element as RIGID BODY that was divided into 396 fine elements of approximate size (20 × 20 × 20) mm as shown in Fig. 11. In analysis, the steel ball was given an initial velocity of 9.87 m/sec.

The four edges of FE models were prevented from translation in both XZ plane and YZ plane (see Fig. 12) while all rotations could simulate the experimental model which was simply supported from all edges. To simulate the motion of the impactor (steel ball), reference point which represent all nodes of impactor are given an initial velocity (9870 mm/s = 9.87 m/s) in a direction perpendicular to slab plane as shown in Fig. 13. Therefore, the impactor struck the slab at a constant velocity mentioned before by falling from constant height which was 4.97m.

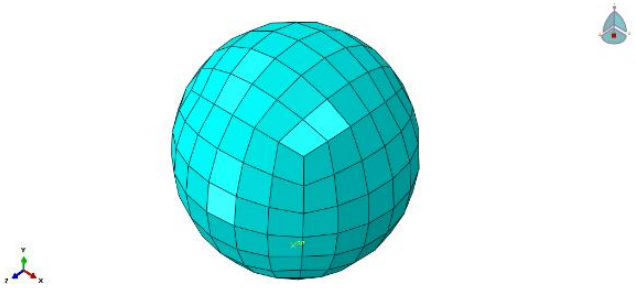

Fig. 11. Modeling of steel ball.

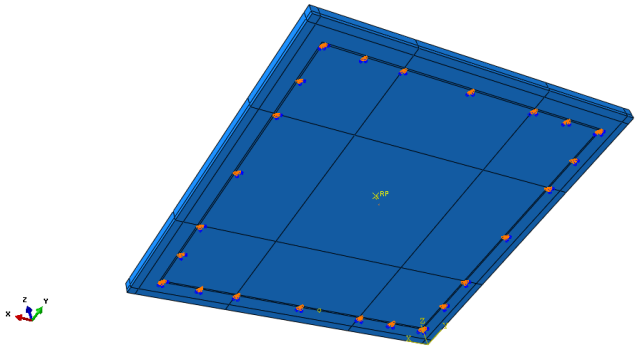

Fig. 12. Boundary condition of FE models.

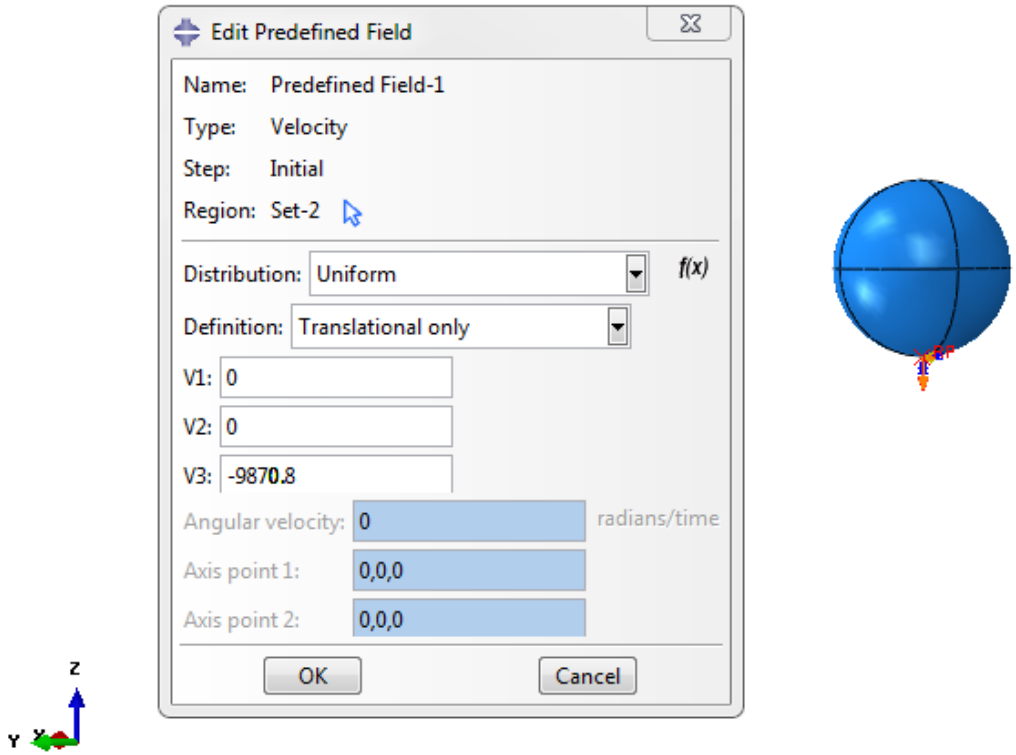

Fig. 13. Initial condition of steel ball.

6. Results Comparison and Discussion

6.1. Mid-point displacement

Displacement of the mid-point of specimen was one of the most important outcomes that has been relied upon in predicting specimen rigidity and strength. Mid-point of specimen was specifically selected as it is the location where the maximum deflection occurred. Fig. 14 illustrates the relationship between time, in milliseconds, and corresponding downward displacement, in millimeters, of the control specimen. The Fig. shows that maximum deflection was 29 mm and occurred after 5.4 milliseconds from impact time. This relationship obtained by converting the video recorded to successive images. Each image had a reading of displacement and was captured at a calculated and specified time from the beginning of the recording. Figs 15 and 16 show initial and maximum displacement as recorded by high frame rate camera during conducting impact test. Actual displacement was calculated by subtracting the initial reading from the maximum reading. Displacement-time relationship obtained by Abaqus for the same slab is shown in Fig. 17. Comparison of maximum values of mid-point displacements for the seven tested specimens obtained experimentally and analytically are presented in Table 9 and Fig. 18.

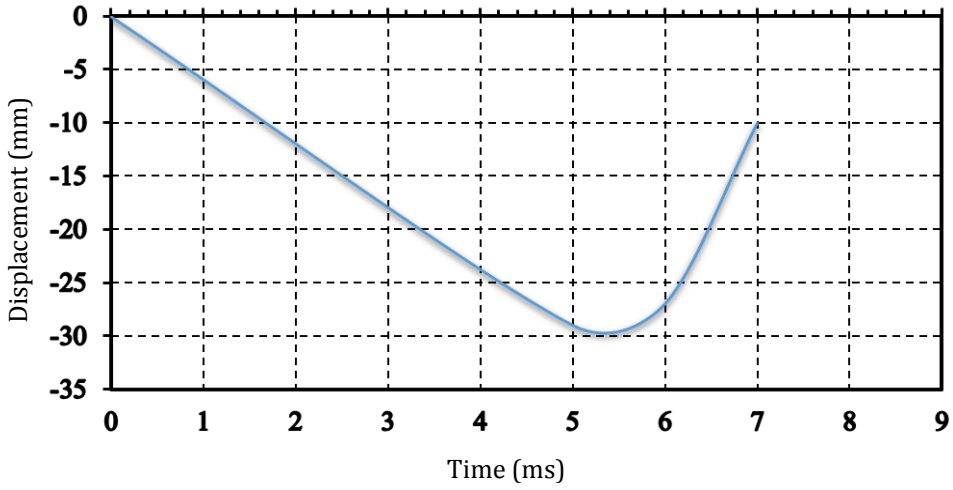

Fig. 14. Displacement versus time in control specimen (S1).

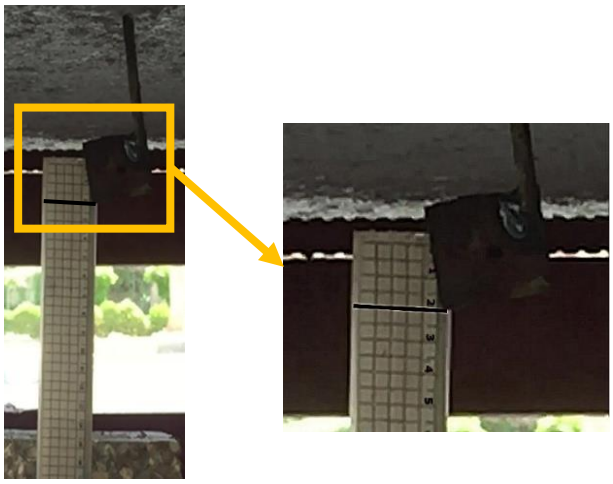

Fig. 15. Initial displacement of S1.

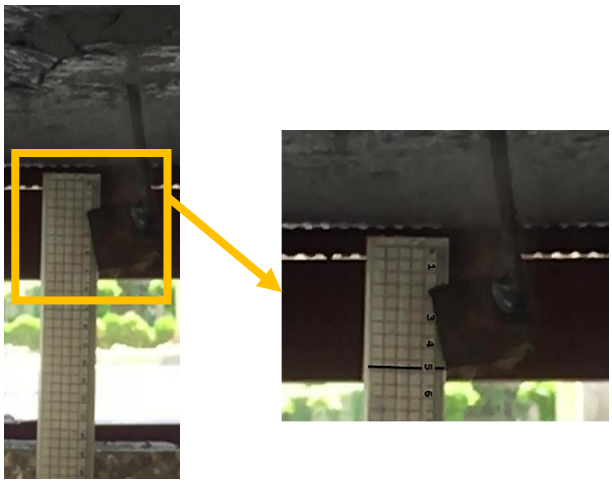

Fig. 16. Maximum displacement of S1.

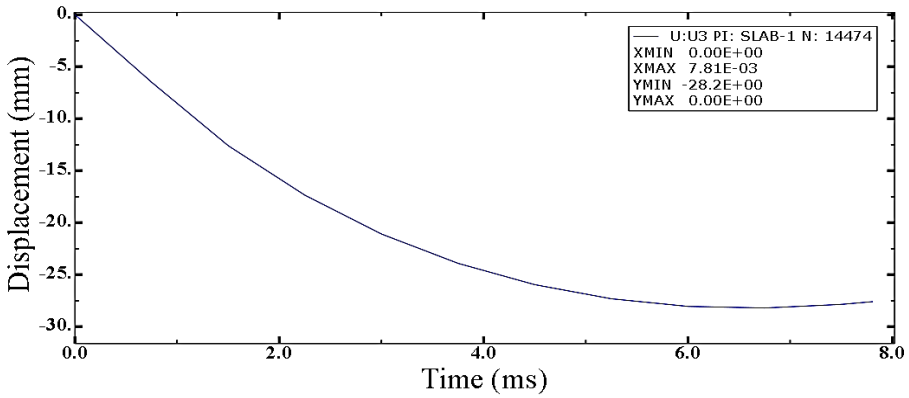

Fig. 17. Deflection- time relationship at mid-point of S1.

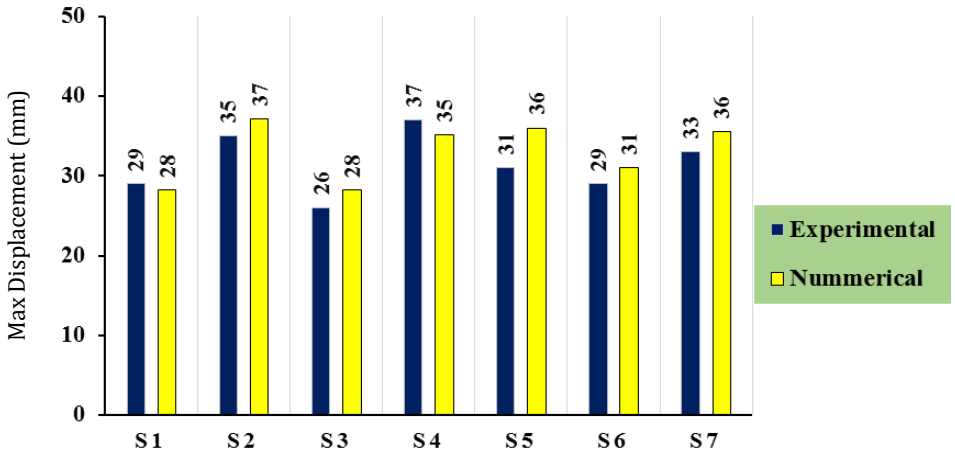

Fig. 18. Max displacements comparison.

Generally, there is a good agreement between experimental and numerical maximum displacement with a mean value of 7% difference. It can be observed that specimens with a square opening (S2, S3, S4) in all cases give closer max displacements to their counterparts with a circular opening (S5, S6, S7) with a difference that didn't exceed 4%, which reducing the effect of the opening shape. The presence of an opening increased the mid-point deflection for S2 and S5, compared to the control specimen, by a mean value of 24%. However, adding expanded metal mesh in (S3 and S6) decreased that ratio to -3.4% and 6.9% respectively. This means that expanded mesh almost eliminated the effect of openings in the tested specimens. In contrast, the effect of adding welded metal mesh in (S4 and S7) did not show a significant effect on reducing the max deflection values. The difference between those specimens and their corresponding specimens without mesh (S2 and S5) did not exceed 5.4%.

Table 9. Comparison between Max displacement results.

No.	Name	Maximum Displacement.		Difference (%)
		Exp.	Num.	
1	S1	29 mm	28.2 mm	2.84 %
2	S2	35 mm	37.1 mm	5.66 %
3	S3	26 mm	28.2 mm	7.80 %
4	S4	37 mm	35.1 mm	5.41 %
5	S5	31 mm	36.0 mm	13.88 %
6	S6	29 mm	31.0 mm	6.45 %
7	S7	33 mm	35.5 mm	7.04 %
		Mean Difference %		7 %

6.2. Cracked pattern

Impact test, as expected, caused crushing in the lower surface of specimens (tension zone) as shown in Fig. 19. Failure zone or crushing zone localized under impact point where concrete has been completely collapsed and then cracks spread gradually by moving away from that zone. Cracks appeared with remarkable width near failure zone and turned into very fine cracks until reaching supports. Failure pattern gives an indication of how the specimen was affected by the impact load, in addition to predict the ability of specimen to absorb impact energy, which contributes in finding some methods that increase the strength of slab and reduce the size of failure zone. Fig. 20 shows the cracked patterns of specimens S2 to S7. Obviously, specimens with added metal mesh, in general, had smaller cracked zones compared to (S2 and S5). Though, specimens with expanded metal mesh (S3, S6) showed the least spread of cracks, which indicates the effectiveness of that type of mesh in controlling crack spread as well as crack width compared to control specimen (S1).

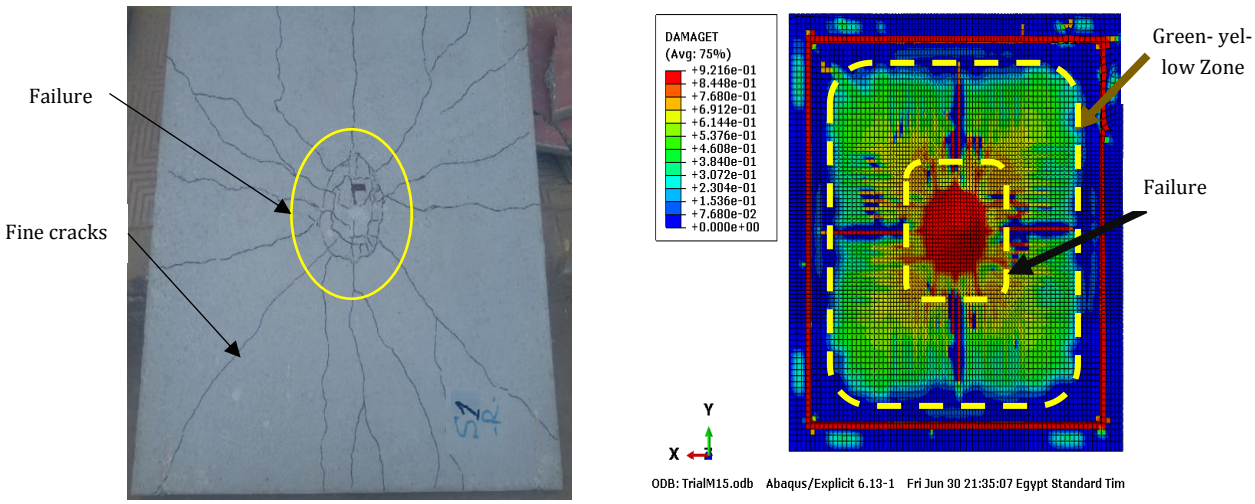

(a) Experimental (b) Finite element

Fig. 19. Cracked pattern of S1.

7. Conclusions

The effect of welded and expanding reinforcing metal mesh on the behavior of slabs with openings under impact loading has been experimentally and numerically investigated in the present study. Seven test specimens; one control, three with circular openings and three with square openings were prepared and tested in Faculty of Engineering, Menoufia University, Egypt. Based on the test results, the following conclusions can be drawn as follows:

- Shape of opening has no significant effect on the behavior of test specimens. The difference in deflection values in specimens with a square opening and their counterparts with a circular opening didn't exceed 4%.

- The presence of opening in the tested specimens without reinforcing mesh resulted in an average ratio of 24% increase in mid-point deflection compared to that of control test specimen. On the other hand, adding metal mesh significantly decreased the above difference to (3.4 to 6.9) %.
- Adding expanded mesh resulted in less displacement values than employing welded mesh. The difference, in some cases, reached 24.3 %.
- Specimens reinforced with metal mesh had smaller cracked zones compared to their counterparts without metal mesh.
- Cracking spread decreased significantly in specimens reinforced by expanded metal.

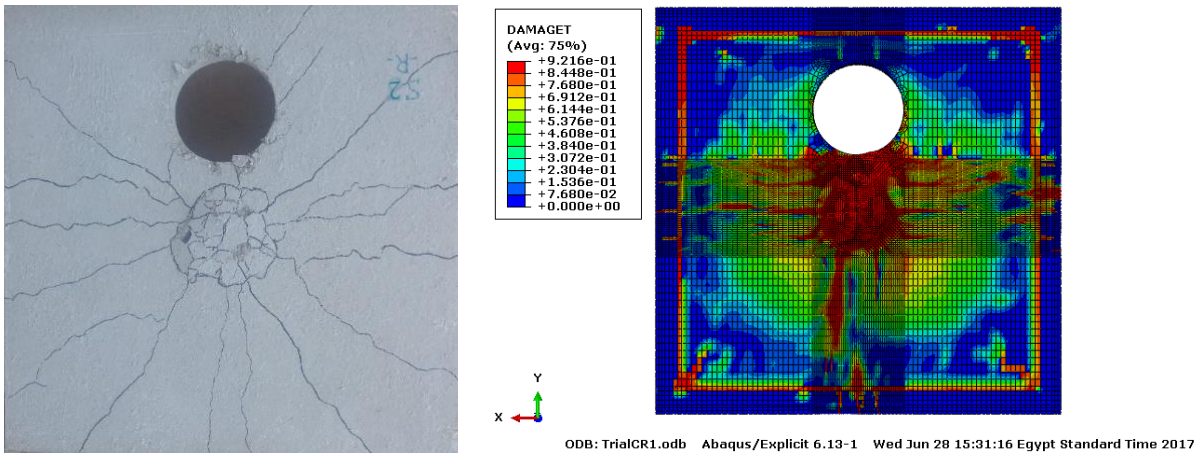

(a) S2

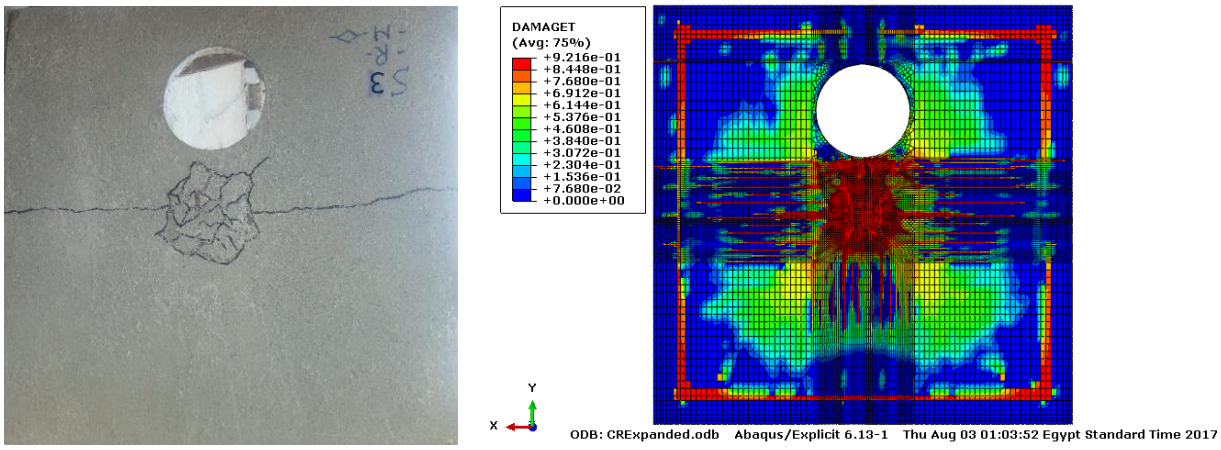

(b) S3

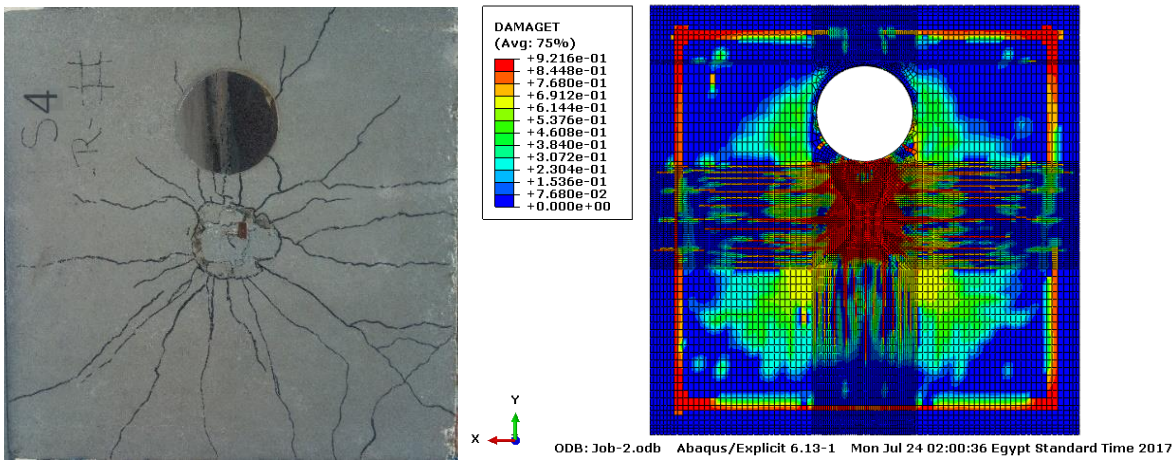

(c) S4

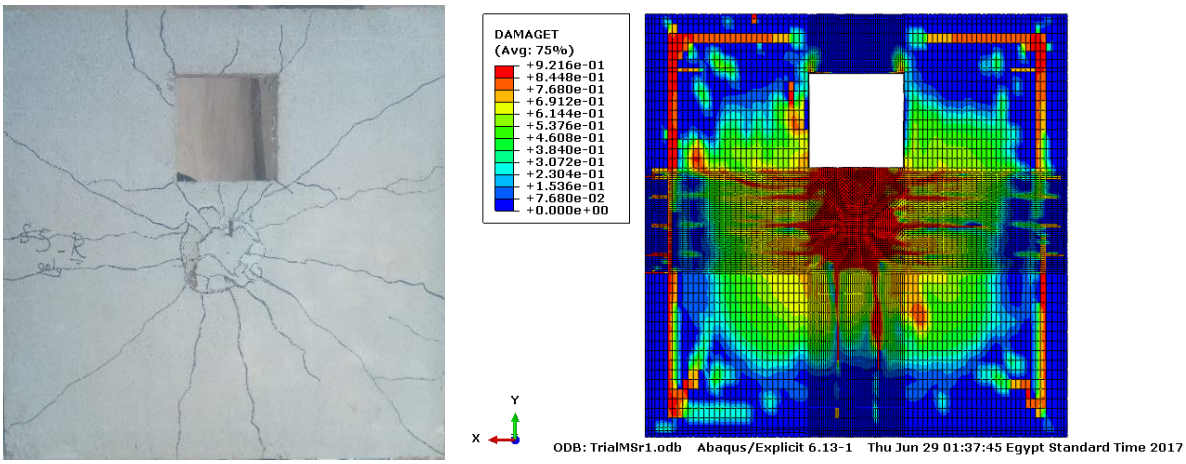

(d) S5

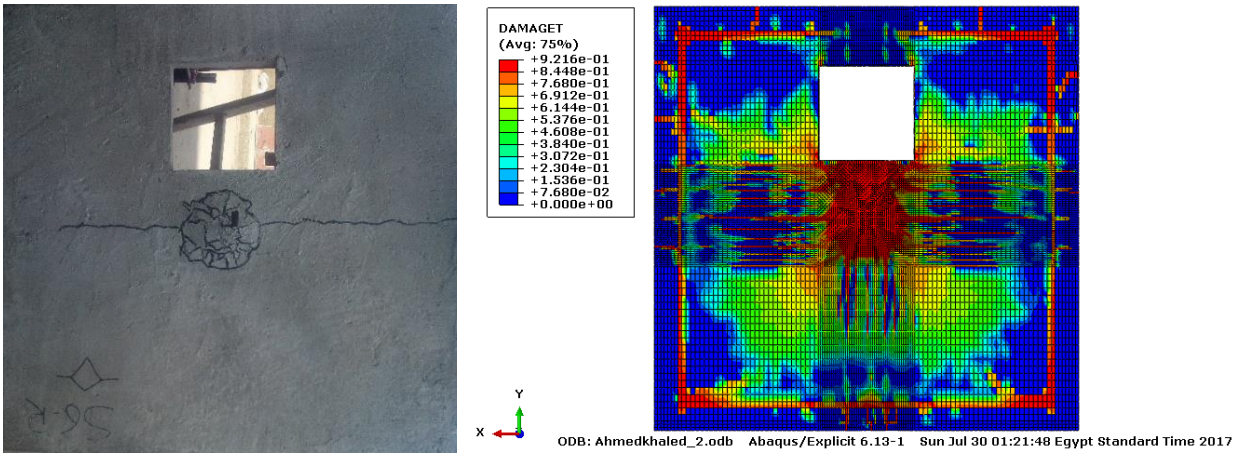

(e) S6

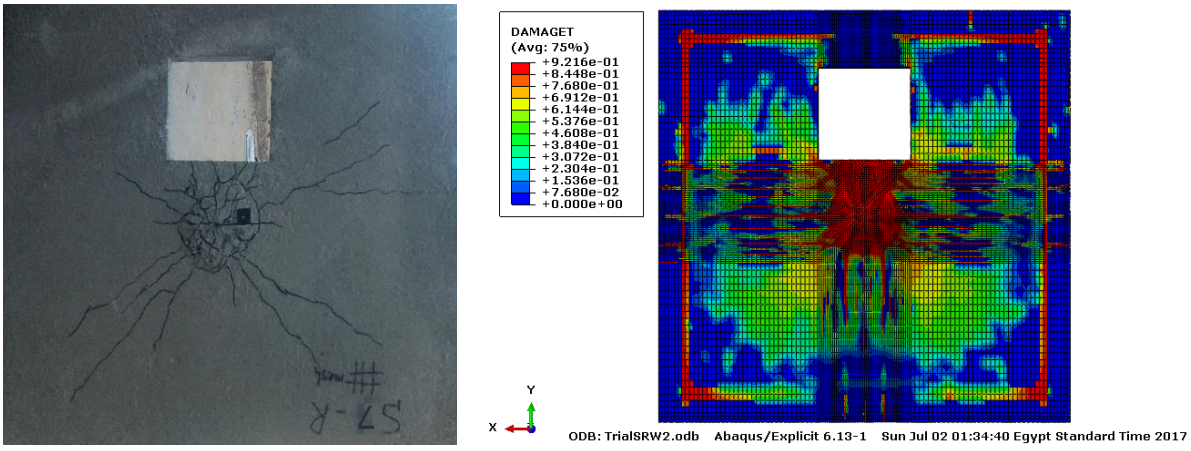

(f) S7

Fig. 20. Cracked patterns of different slabs.

REFERENCES

Abaqus User's Guide (2013). Abaqus Documentation User's Guide. s.l.: Dassault Systems, Simulia Corp.

Ahmed A (2014). Modeling of a reinforced concrete beam subjected to impact vibration using ABAQUS. *International Journal of Civil and Structural Engineering*, 4(3), 227-236.

Ali A, Al-Khafaji A (2015). Nonlinear finite element analysis of reinforced concrete slabs under impact loads. *Journal of Kerbala University*, 13(1), 247-269.

Andersson A (2014). Impact Loading on Concrete Slabs. Experimental Tests and Numerical Simulations. *Report*, KTH Royal Institute of Technology, Stockholm, Sweden.

Antunes, G, Masuero Â (2016). Flexural tensile strength in mortar coating reinforced with different types of metal mesh, a statistical comparison. *Construction and Building Materials*, 121, 559-568.

Attallah E (2012). Analysis of Reinforced Concrete Structures Subjected to Impact Loads. *M.Sc. thesis,* Department of Civil Engineering, Menoufia University, Egypt.

Batarlar B (2013). Behavior of Reinforced Concrete Slabs Subjected to Impact Loads. *M. Sc. thesis*, İzmir Institute of Technology, Turkey.

Boon K, Diah A, Loon L (2009). Flexural Behaviour of reinforced concrete slab with Opening, Proceedings of MUCEET2009, *Malaysian Technical Universities Conference on Engineering and Technology*, June 20-22, MS Garden, Kuantan, Pahang, Malaysia

ECP 203 (2007). Egyptian code of practice for design and construction of concrete structures. National Center of Housing and Building researches, Cairo, Egypt.

Elavenil S, Knight G (2012). Impact response of plates under drop weight. Impact testing. *Daffodil International University Journal of Science and Technology*, 7(1), 1-11.

EOS1658-4/2008 (2008) Testing of concrete, Part 3, Making and curing test specimens (ISO 1920-3:2004). International Organization for Standardization.

Khajehdehi R, Panahshahi N (2014). Nonlinear FE analysis of RC building floor diaphragms with openings subjected to in-plane and out-of-plane loads, *Tenth U.S. National Conference on Earthquake Engineering, Frontiers of Earthquake Engineering*, July 21-25, Anchorage, Alaska

Kishi N (2004). Practical methods for impact test and analysis. Structural Engineering Series, *JSCE, impact problems*, No.15. (In Japanese).

Mokhatar S, Abdullah R (2012). Computational analysis of reinforced concrete slabs subjected to impact loads. *International Journal of Integrated Engineering*, 220(4), 70-76.

Saatci S, Vecchio F (2009). Nonlinear finite element modeling of reinforced concrete structures under impact loads. *ACI Structural Journal*, 106 (5), 717-725.

Selim H, Seracino R, Sumner, Smith S (2011). Case study on the restoration of flexural capacity of continuous one-way RC slabs with cut-outs. *ASCE Journal of Composites for Construction*, 15(6), 992–998.

Shaheen Y, Abusafab H (2017). Structural behavior for rehabilitation ferrocement plates previously damaged by impact loads. *Elsevier Case Studies in Construction Materials*, 6, 72-90.

Shaheen Y, Hekal G, Khalid A (2017). Behavior of reinforced concrete slabs with openings under impact loads. *Menoufia University, Faculty of Engineering, First International Conference*, 24 -28 March, Sharm Elsheikh, Egypt.

Sudarsana R, Sashidhar C, Vaishali G, Venkata R (2015). Behavior of high performance concrete two-way slabs in impact for fixed edge condition. *International Journal of Emerging Trends in Engineering and Development*, 2(5), 105-111.

Tahmasebinia F (2008). Numerical Modeling of Reinforced Concrete Slabs Subjected to Impact Loads. *M.Sc. thesis*, Department of Civil Engineering, University of Wollongong New South Wales, Australia.

Tahmasebinia F, Remennikov A (2008). Simulation of the reinforced concrete slabs under impact loading. *Australasian Structural Engineering Conference (ASEC)*, 26–27 June, Melbourne, Australia.

Thilakarathna H, Thambiratnam D, Dhanasekar M, Perera N (2009). Behavior of axially loaded concrete columns subjected to transverse impact loads. *34th Conference on Our World in Concrete & Structures*, 16–18 August, Singapore.

Yoo D, Min K, Lee J, Yoon Y (2012). Enhancing impact resistance of concrete slabs strengthened with FRPS and steel fibers. *6th International Conference on FRP Composites in Civil Engineering*, Rome, Italy.

Challenge Journal of Concrete Research Letters

Research Article

Prediction of self compacted rubberized concrete properties using Taguch methods

Mohamed Safaan, Fatma M. Eid *, Amal A. Nasser, Mohamed Emara

Department of Civil Engineering, Menoufia University, Shebin ElKoum, Menofia, Egypt

ABSTRACT

The effect and optimization of using self-compacting rubberized concrete was investigated by using Taguchi method. Design of experiment was performed via orthogonal array to accommodate four factors with four levels. These factors were the percentage of fine rubber, coarse rubber, fly ash and viscocrete in the concrete mix. The signal-to-noise (S/N) ratio and the analysis of variance (ANOVA) were employed to study the performance characteristics of self-compacting rubberized concrete (SCRC). Rubberized concrete can be improved using the concrete proportioned as self-compacting concrete. The results indicate that there was a reduction in the strength with increasing rubber content but there was an increase in impact resistance. However, the replacement of 10% of coarse aggregate with coarse rubber gave more strength than that of zero rubber mix by 124% at 90 days. Replacement of 20% of both fine and coarse aggregates with fine and coarse rubber respectively, increased impact resistance by 453% compared to the corresponding SCRC control mix.

ARTICLE INFO

Article history:
Received 10 February 2018
Accepted 29 May 2018

Keywords:
Rubber
Recycling
Self-compacting concrete
Taguchi method
ANOVA

1. Introduction

Self-Compacting Concrete (SCC) is a sophisticated high performance concrete (Taha et al., 2008) described as the ''most revolutionary step'' in concrete technology over the last two decades due to its impact on economic and environmental sustainability in the construction industry (Ouchi and Okamura, 2003). It offers the advantages of increased productivity rates, decreased manpower, and elimination of the noise and fuel consumption associated with vibrator plant (Ouchi and Okamura, 1999). In comparison with plain concrete, it has the ability to fully self-compact under its own weight and has high flowability and filling rates, reduced blocking in congested reinforced areas, and high segregation resistance, as well as high durability, low permeability and high compressive strength (Bignozzi and Sandrolini, 2006).

Solid waste disposal is a major environmental issue on cities around the world (Najim and Hall, 2012). The volume of polymeric waste like tyre rubber is increasing. The waste tyre rubber becomes an environmental problem due to its non-biodegradable nature. Up to now a small part is recycled and millions of tyres are just stockpiled; land filled or buried and used as fuel in many industries. Recycling end-of-life vehicle tyres as alternative aggregates to produce a new class concrete is an innovative option with environmental, economic and performance benefits (Najim and Hall, 2012).

Many researchers have therefore used rubber particles as aggregates in concrete production to eliminate poor deformation capacity, low tensile strength, and improve energy absorption capacity. Aggregate rubber particles enhanced deformation and energy absorption capacities while they decreased workability and mechanical properties (Mishra and Panda, 2015). Self-compacting rubberized concrete (SCRC) was produced to diminish the negative effect of rubber aggregate on the mechanical properties and workability of concrete (Khalil et al., 2015). Due to the high powder content of SCC its microstructure is very compacted and dense, which results in high mechanical strength and brittle failure modes. Therefore, (SCRC) composites could be used for applications requiring deformable (high ductility

* *Corresponding author*. E-mail address: fatma_elzahraa2002@yahoo.com (F. M. Eid)
ISSN: 2548-0928 / DOI: https://doi.org/10.20528/cjcrl.2018.02.002

concrete with high flowability and low/medium strength (<35 MPa), which is difficult to achieve using SCC using alternative aggregates that are environmentally friendly (sustainable concrete). In infrastructure applications the range of strength is usually between 28 and 35 MPa. In applications such as bridge barriers and road foundations, concrete with high deformation and high toughness is desirable while >35 MPa compressive strength is not required (Najim and Hall, 2012).

2. Aim of the Research

In the current research fresh and harden properties of (SCRC) were investigated using Taguchi method. Sixteen different concrete mixes were designed with the same water/powder ratio W/P (P=cement+fly ash). Their self-compacting characteristics and final mechanical behavior are reported and discussed.

3. Parameter Design Methodology

Taguchi's parameter design method is a powerful tool for optimizing the characteristic performance of a product/process. Optimization quality characteristic minimizes Sensitivity to Noise (S/N) (uncontrollable) factors. In the present study, four control factors were chosen with four levels as shown in Table 1.

3.1. Design of experiment

The experiment was designed based on the orthogonal array technique. An orthogonal array is a fractional factorial design. It is obtained by assigning the selected factors and their levels to appropriate columns of L16 orthogonal array. This array has 16 rows and 4 columns, each row represents a trial condition and each column accommodates a specific process parameter. The main effects can be estimated. The numbers in each column indicate the levels of specific factors (A, B, C and D). Taguchi Orthogonal Array Design is L16 (4**4). Factors are 4. Runs are 16 (Ghazy, 2012, 2015; Zahran and Nasser, 2014).

3.2. Taguchi's orthogonal array approach of experimental design

Taguchi's target is developing products that achieve the target value on a consistent basis. The variation around the target value should be minimized. In other words, quality is achieved by minimizing the deviation from the target. Factors and levels are illustrated in Table 1; the mixes are given in Table 2. Factor A is replacement of fine aggregates by fine rubber (1mm) (replaced by 0, 10, 15 and 20%). Factor B is replacement of coarse aggregates by coarse rubber (5mm) (replaced by 0, 10, 15 and 20%). Factor C is addition of fly ash as a ratio of cement (added by 20, 25, 30, and 35%). Factor D is using superplasticizer (viscocrete) as a ratio of cement (2.00, 2.25, 2.50 and 2.75%) (Zahran and Nasser, 2014).

Table 1. Control factors of the experimental work.

Level	Factors			
	A Replacement of fine aggregates by fine rubber	B Replacement of coarse aggregates by coarse rubber	C Fly-ash (cement %)	D Viscocrete (cement %)
1	0 %	0 %	20 %	2.00 %
2	10 %	10 %	25 %	2.25 %
3	15 %	15 %	30 %	2.50 %
4	20 %	20 %	35 %	2.75 %

Table 2. Experimental test design of control factors with factor levels.

Exp. No.	Factors			
	% Replacement by volume of aggregate		Addition (% wt. of cement)	
	Fine rubber	Coarse rubber	Fly ash	Viscocrete
1	0	0	20	2.00
2	0	10	25	2.25
3	0	15	30	2.50
4	0	20	35	2.75
5	10	0	25	2.50
6	10	10	20	2.75
7	10	15	35	2.00
8	10	20	30	2.25
9	15	0	30	2.75
10	15	10	35	2.50
11	15	15	20	2.25
12	15	20	25	2.00
13	20	0	35	2.25
14	20	10	30	2.00
15	20	15	25	2.75
16	20	20	20	2.50

4. Materials and Methods

All test specimens were fabricated using locally available materials.

Cement: A locally produced ordinary Portland cement (42.5N) produced by Lafarge Company meeting the requirement of E.S. 373/2003 was used with constant content (400 kg/m^3) for all mixes.

Fly ash: Sika fly ash type P from Sika Egypt Company (El Obour factory) was used as addition to cement.

Fine Aggregates: The sand used was local natural siliceous sand with fineness modulus 2.77 and specific gravity 2.64.

Coarse Aggregates: Coarse aggregates used was natural crushed limestone with maximum aggregate size of 12 mm to achieve the requirement of self-compacting concrete.

Superplasticizer: A high range water reducer without retarding was used. (Sika viscocrete 3425) was used as a demand for producing SCC. It meets the requirements for superplasticizers according to ASTM-C- 494 Types G and F and BS EN 934 part 2: 2001.

Fine rubber aggregates: The fine crumb rubber used in this research is produced by MARSO factory at 10th Ramadan city-Egypt with size of (1mm) and was used as a partial replacement (by volume) of fine aggregate, (see Fig. 1).

Coarse rubber aggregates: The coarse rubber used in this research is produced by MARSO factory at 10th of Ramadan city-Egypt with one size of (5mms) and was used as a partial replacement (by volume) of coarse aggregate, (see Fig. 1).

Water: Fresh tap water was used with water/binder ratio w/b = 0.37

5. Mix Contents and Procedure

Mix contents: the cement content was constant at 400 kg/m^3 for all mixes with water/binder ratio of 0.37 and the mix proportion ratio (of weight) for cement: sand: dolomite was 1:2.125:2.125 respectively (binder = cement + fly ash).

Mixing procedure: was carried out in three stages; dry mix for 2 min, adding 75% of (water+S.P) and mixing for 2 min and a final mix for not less than 3 min after adding the remaining amount of (water+S.P). Subsequently, the fresh properties of SCRC mixes; Flowability and Passing-ability tests (slump flow, T50, V-Funnel and J-Ring) were determined. Concrete specimens were cast in standard steel molds. After 24 h from mixing, all the specimens were de-molded and cured in wet canvas for 7 days.

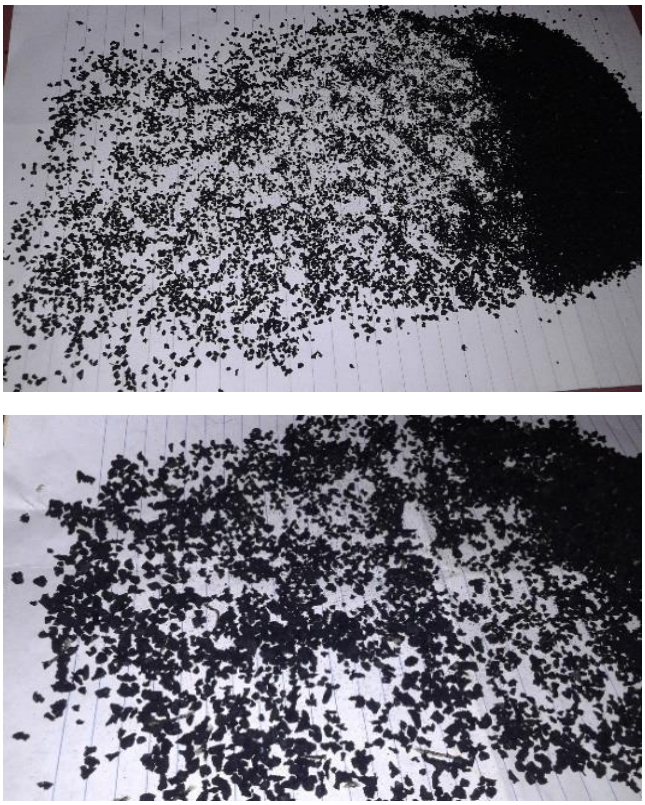

Fig. 1. Fine and coarse rubber.

6. Tests

6.1. Fresh tests

Fresh tests were performed according to the procedure recommended by EFNARC committee (European Federation for Specialist Construction Chemicals and Concrete Systems) (EFNARC (2005). See Fig. 2.

6.1.1. Slump flow test

Slump flow value describes the flowability of a fresh mix in unconfined conditions. It is a sensitive test that can normally be specified for all self-compacting concretes, as the primary check that the fresh concrete consistence meets the specification (Erhan, 2010). See Fig. 2.

6.1.2. V-Funnel:

When performing the V-Funnel test, a V shaped funnel is filled with fresh concrete and the time taken for the concrete to flow out of the funnel is measured and recorded as the V-Funnel flow time, see Fig. 2.

6.2. Hardened SCRC

6.2.1. Compressive strength test

Test was carried out on 15*15*15 cm cubes and according to ASTM C39-86. The capacity of the compression machine used is 2000 KN.

6.2.2. Impact test

Beams 10*10*50 cm were prepared for this test. The impact resistance was assessed by measuring the ability of concrete specimens to withstand repeated blows of a free failing load (3kg) at a constant travelling height of 40 cm above the midpoint of the tested concrete beam which was supported on two ends. The load was then left to fall freely on the top side of the concrete beam and the number of impact blows to cause failure was recorded (Eid, 2003; Taha et al., 2003; Najim and Hall, 2012).

Fig. 3 shows the hardened tests set up.

(a) Slump flow test (b) V-Funnel test

Fig. 2. Fresh tests.

(a) Compression test (b) Impact test

Fig. 3. Hardened tests.

7. Results

7.1. Fresh properties

Experimental test results of fresh properties for slump flow and V-Funnel tests for SCRC are shown in Table 3.

7.2. Hardened properties

Experimental test results of compressive strength for SCRC are shown in Table 4. Table 5 shows test results for impact resistance which represented by numbers of blows.

8. Analysis and Discussion

Design of experiment data is used to analyze the mean response function. In Taguchi technique, the variation of the response is examined using an appropriately chosen S/N ratio. This ratio is the mean (signal) to the standard deviation (noise). The ratios, derived from the quadratic loss function, are expressed on a decibel (dB) scale. The formula used to compute the S/N ratio depends on the objective function. Generally, three standard S/N equations are widely used to classify the objective function as: 'larger the better', 'smaller the better', or 'nominal the best'. Focusing on the strength characteristic, a larger S/N ratio is always desirable.

Table 3. Experimental test results (fresh properties).

Mix. No.	Slump (mm)	V-Funnel (sec.)	Mix. No.	Slump (mm)	V-Funnel (sec.)
1	723	3.65	9	675	13.94
2	735	3.79	10	690	7.20
3	755	3.56	11	550	18.25
4	720	6.47	12	585	14.97
5	710	7.81	13	665	6.16
6	740	5.89	14	630	11.03
7	715	6.71	15	605	17.53
8	645	5.72	16	560	9.22

Table 4. Compressive strength test results (hardened properties).

Mix. No.	Compressive strength (MPa)			Mix. No.	Compressive strength (MPa)		
	7days	28days	90days		7days	28days	90days
1	33.2	47.7	52.0	9	22.1	31.6	44.5
2	40.3	53.3	64.4	10	21.3	32.9	37.3
3	27.6	37.7	44.4	11	20.4	24.8	32.2
4	21.6	347	456	12	19.0	24.3	29.0
5	28.4	421	483	13	23.0	38.4	32.2
6	23.9	35.8	43.9	14	23.9	25.7	33.6
7	21.9	33.2	41.2	15	20.8	24.8	30.2
8	20.2	26.0	38.3	16	18.3	20.2	29.8

Table 5. Impact test results.

Mix. No.	Impact (blows) 28 days	Mix. No.	Impact (blows) 28 days
1	17	9	23
2	13	10	21
3	15	11	31
4	15	12	31
5	29	13	35
6	23	14	54
7	22	15	55
8	22	16	77

In the present study, compressive and impact resistance are a 'larger is better' type of quality characteristic since the goal is to maximize the strength. The standard S/N ratio computing formula for this type of response is:

$$\left(\frac{S}{N}\right)_i = -10 \log\left[\frac{1}{n}\sum_{j=1}^{n}\frac{1}{Y_{ij}^2}\right]. \quad (1)$$

V-Funnel is a 'smaller is better' type of quality characteristic since the goal is to minimize them. The standard S/N ratio computing formula for this type of response is:

$$\left(\frac{S}{N}\right)_i = -10log\left[\frac{1}{n}\sum_{j=1}^{n} Y^2\right], \quad (2)$$

where '*i*' is the number of a trial; 'Y_{ij}' is the measured value of quality characteristic for the ith trial and jth experiment; '*n*' is the number of repetitions for the experimental combination. Signal-to-noise ratios are computed using Eq. (1) for each experimental condition for compressive and impact resistance. The factor effects can be separated out in terms of S/N ratio.

The analysis of variance (ANOVA) is also performed to study the relative significance of the process parameters. The contributions of the various parameters are quantified.

8.1. Fresh properties

The filling ability and stability of SCRC in the fresh state can be defined by four key characteristics namely flowability, viscosity, passing ability, and segregation

resistance. Each characteristic can be addressed by one or more test methods (EFNARC, 2005). For instance, flowability can be measured via slump flow test, viscosity can be measured through the V-Funnel flow time tests.

Self-compacting concrete requirements in the fresh state that are appropriate for a given application should be selected from one or more of above mentioned four key characteristics and then specified by class or target value. To define the flowability, viscosity, passing ability, and segregation resistance of the produced SCRC, slump flow diameter and V-Funnel flow time of the all produced concretes were measured and presented.

8.1.1. Slump flow test

The average values of S/N ratios of the control factors for slump flow test are shown in Table 6 and Fig. 4. Table 7 shows the analysis of variance for this test. Increasing rubber content decreased slump flow diameter but increasing fly ash and/or viscocrete increased slump flow diameter. Addition fly ash to the mix increased cement paste volume which made the mix more flowability. Viscocrete increased the viscosity of concrete which increased the slump flow diameter.

Table 6. Response of signal to noise ratios for slump flow (larger is better).

Level	Fine rubber (A)	Coarse rubber (B)	Fly ash (C)	Viscocrete (D)
1	57.30	56.81	56.08	56.40
2	56.92	56.87	56.33	56.20
3	55.88	56.27	56.58	56.58
4	55.76	55.91	56.87	56.69
Delta	1.54	0.96	0.78	0.49
Rank	1	2	3	4

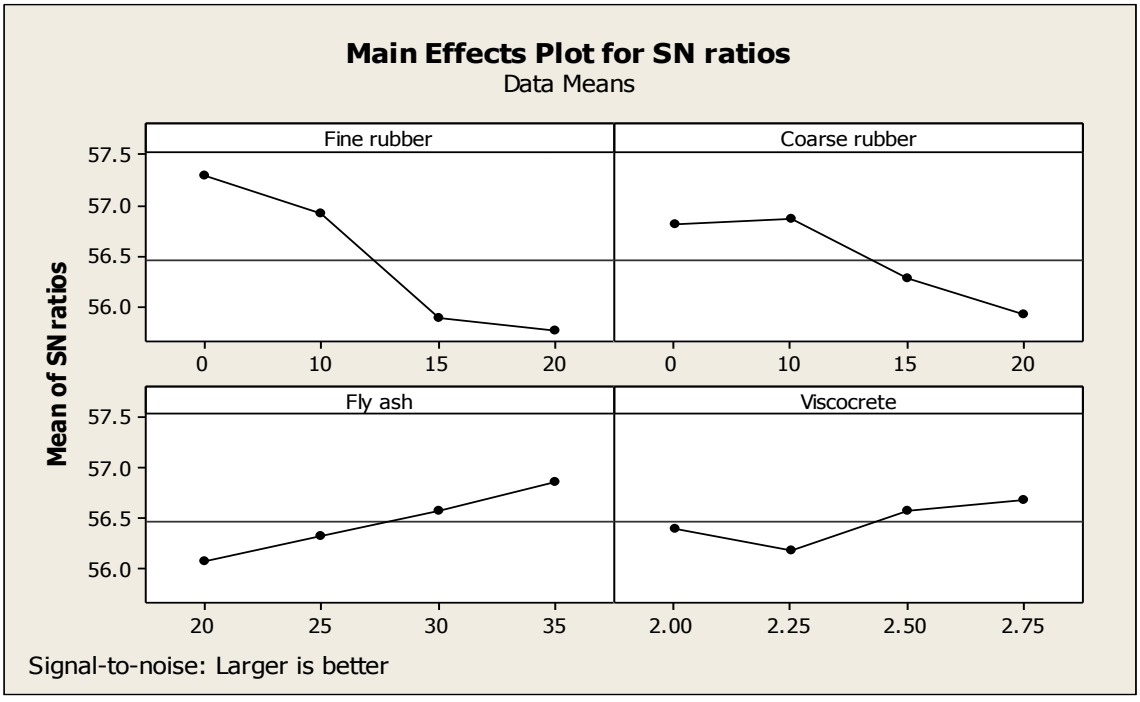

Fig. 4. Main effect plot for signal to noise ratio of slump flow (larger is better).

Table 7. Analysis of variance for slump flow test, using adjusted SS for tests.

Source	DF	Seq SS	Adj SS	Adj MS	Contribution %
Fine rubber	3	40344.9	40344.9	13448.3	61.27
Coarse rubber	3	13407.4	13407.4	4469.1	20.36
Fly ash	3	6557.4	6557.4	2185.8	9.96
Viscocrete	3	3182.4	3182.4	1060.8	4.83
Error	3	2344.9	2344.9	781.6	3.56
Total	15	65837.1			100

8.1.2. V-Funnel test

As mentioned above, V-Funnel test is measuring the viscosity like T50 test. But here, viscocrete has 2nd rank in S/N analysis which mean that it has a big effect on V-Funnel test. However, using the highest content of viscocrete (2.75%) increased the time of this test as shown in Fig. 5. like T50, increasing rubber content increased V-Funnel time. The average values of S/N ratios of the control factors for this test are shown in Table 8 and Fig. 5. Table 9 shows the analysis of variance for this test.

Table 8. Response of signal to noise ratios for V-Funnel (smaller is better).

Level	Fine rubber (A)	Coarse rubber (B)	Fly ash (C)	Viscocrete (D)
1	-12.52	-16.94	-17.79	-18.03
2	-16.23	-16.24	-19.45	-16.93
3	-22.19	-19.42	-17.48	-16.33
4	-20.20	-18.54	-16.42	-19.85
Delta	9.67	3.17	3.03	3.51
Rank	1	3	4	2

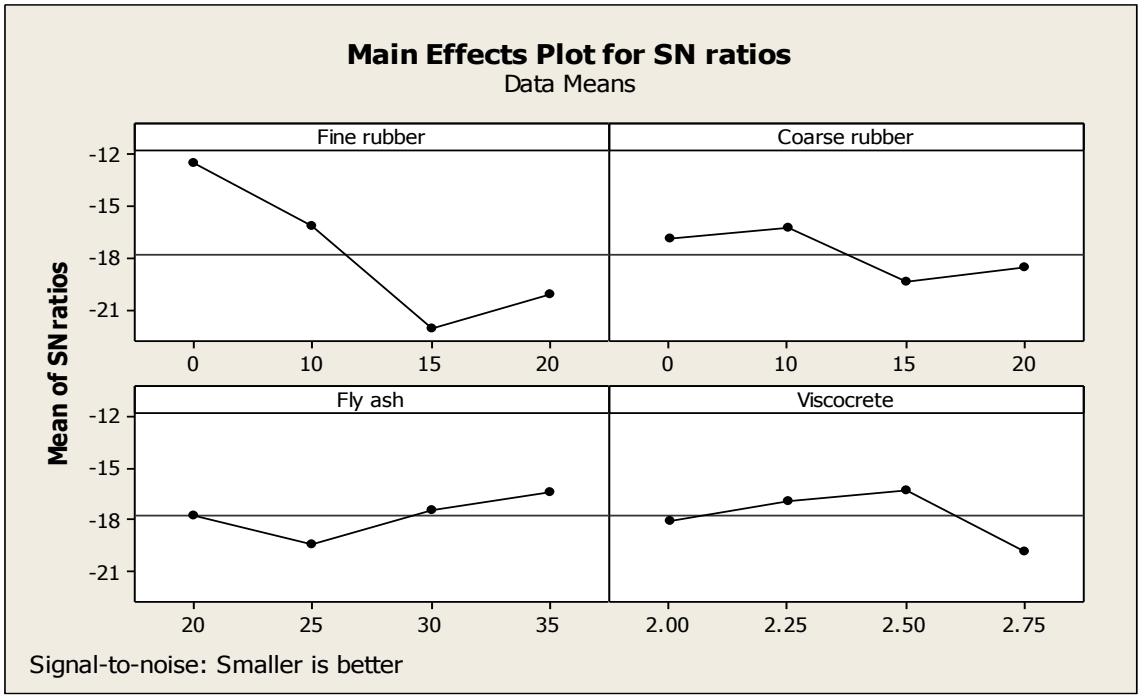

Fig. 5. Main effect plot for signal to noise ratio of V-Funnel results (smaller is better).

Table 9. Analysis of variance for V-Funnel test, using adjusted SS for tests.

Source	DF	Seq SS	Adj SS	Adj MS	Contribution %
Fine rubber	3	209.952	209.952	69.984	59.57
Coarse rubber	3	46.302	46.302	15.434	13.13
Fly ash	3	39.520	39.520	13.173	11.21
Viscocrete	3	33.017	33.017	11.006	9.36
Error	3	23.628	23.628	7.876	6.70
Total	15	352.419			100

8.2. Hardened properties

The mean of three tested values at 28 days was recorded to determine the compressive and impact resistance for all mixtures.

8.2.1. Compressive strength

It was found that increasing rubber content decreased the compressive strength. The deterioration in compressive strength can logically be attributed to (i) the low

modulus of elasticity (E) for rubber particles and high Poisson ratio (v) which may encourage premature cracking under load, (ii) increased porosity due to air entrainment from rubber particles, and (iii) weak bonding in the interfacial transition zone between the cement paste and rubber particles which could be due to crack initiation from the voids that form between crumb rubber particles and cement paste. Therefore, under compression loading the aggregates can be susceptible to pullout resulting in particle perimeter voids and crack initiation sites. For fly ash, increasing fly ash content increased compressive strength as it works as a filler which fills the voids on concrete. Using 35% of fly ash as addition to the mix gave highest compressive strength. Viscocrete has small effect on compressive strength. It had the 4th rank in S/N analysis. But the addition of super plasticizer in SCC gives more strength in early age.

The average values of S/N ratios of the control factors for compressive strength test are shown in Table 10 and Fig. 6. Table 11 shows the analysis of variance for this test.

Table 10. Response of signal to noise ratios for compressive strength of 28 days (larger is better).

Level	Fine rubber (A)	Coarse rubber (B)	Fly ash (C)	Viscocrete (D)
1	52.62	51.93	49.66	49.98
2	50.57	51.04	50.65	50.60
3	48.98	49.43	49.50	50.12
4	48.46	48.23	50.82	49.94
Delta	4.15	3.70	1.32	0.66
Rank	1	2	3	4

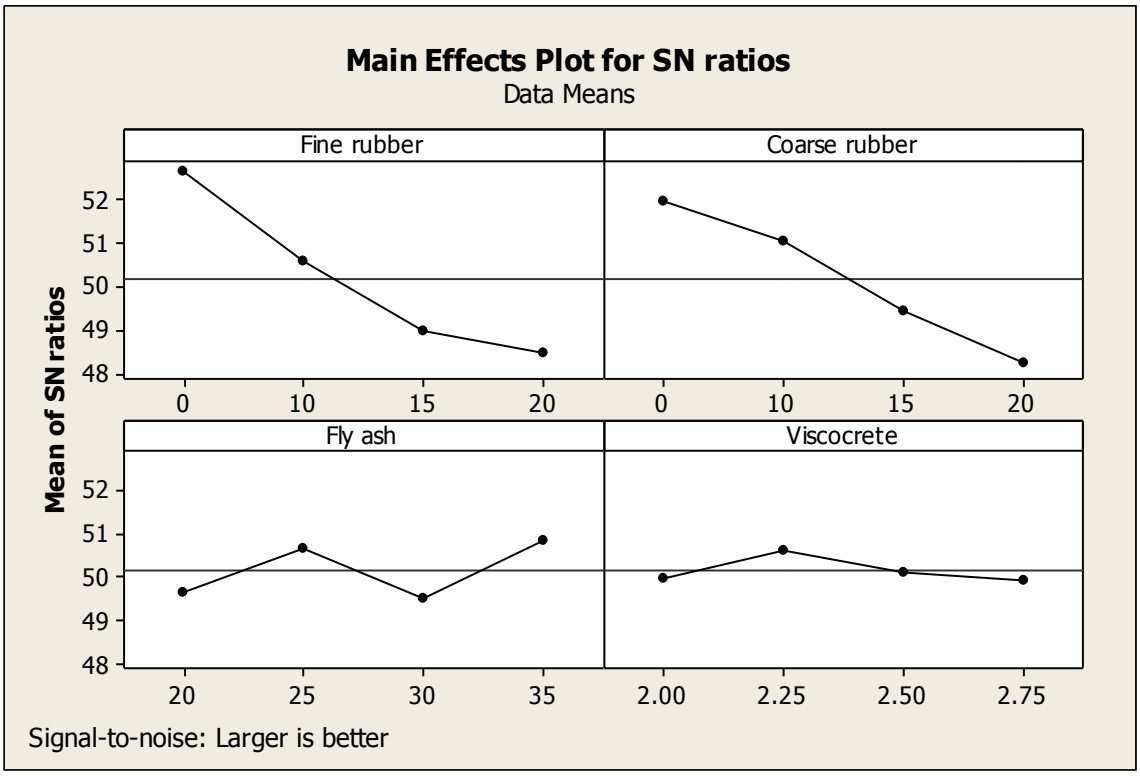

Fig. 6. Main effect plot for signal to noise ratio of compressive strength after 28 days (larger is better).

Table 11. Analysis of variance for 28 days compressive strength, using adjusted SS for tests.

Source	DF	Seq SS	Adj SS	Adj MS	Contribution %
Fine rubber	3	65266	65266	21755	52.098
Coarse rubber	3	46506	46506	15502	37.12
Fly ash	3	8413	8413	2804	6.71
Viscocrete	3	3273	3273	1091	2.61
Error	3	1818	1818	606	1.45
Total	15	125275			100

8.2.2. Impact resistance

Increasing rubber content led to increase impact resistance. The impact resistance, as a number of blows, increased from 17 blows for mix No.1 (no rubber replacement) to 77 blows for mix No.16 (20% fine rubber and 20% coarse rubber). This gain of impact resistance of SCRC is due to the ability of rubber particles to absorb the plastic energy, which generated from the falling of a mass from a certain height. In addition, the high deflection of the rubberized concrete increases the ability to withstand more energy. Table 12 and Fig. 7 show the average values of S/N ratios of the control factors for T50 test. The analysis of variance for this test is shown in Table 13. The percentage of fine rubber replacement was the most significant parameter influencing the impact resistance. The percentage contribution was 75.14%.

Table 12. Response of signal to noise ratios for impact resistance after 28 days (larger is better).

Level	Fine rubber (A)	Coarse rubber (B)	Fly ash (C)	Viscocrete (D)
1	23.06	27.01	29.99	29.09
2	28.24	28.11	28.82	27.70
3	28.57	28.96	28.45	28.69
4	34.35	30.15	26.97	28.75
Delta	11.29	3.14	3.03	1.39
Rank	1	2	3	4

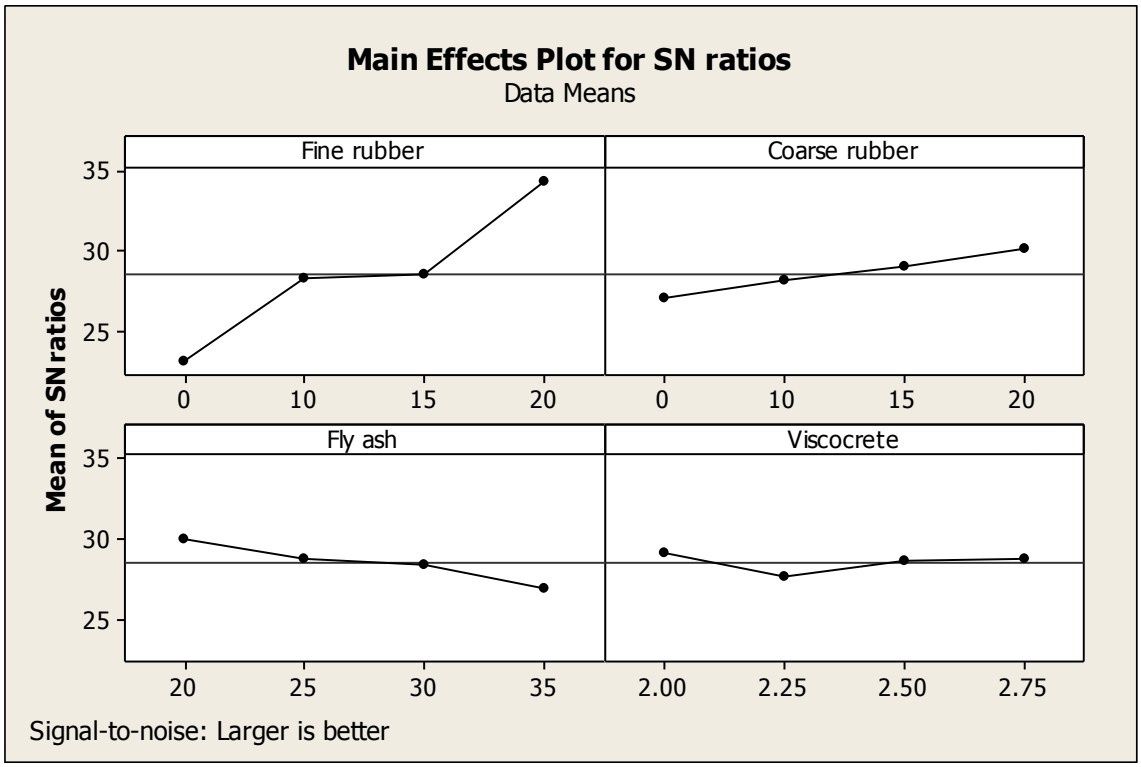

Fig. 7. Main effect plot for signal to noise ratio of impact resistance after 28 days (larger is better).

Table 13. Analysis of variance for 28 days impact resistance, using adjusted SS for tests.

Source	DF	Seq SS	Adj SS	Adj MS	Contribution %
Fine rubber	3	3514.35	3514.35	1171.45	75.14
Coarse rubber	3	467.47	467.47	155.82	10
Fly ash	3	443.13	443.13	147.71	9.47
Viscocrete	3	146.41	146.41	48.80	3.13
Error	3	105.24	105.24	35.08	2.25
Total	15	4676.60			100

9. Prediction of Optimum Quality Characteristic

The predicted mean of the quality characteristic for slump flow, V-Funnel, compressive strength and impact resistance is computed using the following equation:

$$S_{mp} = \bar{Y} + (\bar{A}_0 - \bar{Y}) + (\bar{B}_0 - \bar{Y}) + (\bar{C}_0 - \bar{Y}) + (\bar{D}_0 - \bar{Y}) + (\bar{E}_0 - \bar{Y}) . \quad (3)$$

It is the grand average of performance characteristic.

$$(\bar{A}_0 - \bar{Y}), (\bar{B}_0 - \bar{Y}), (\bar{C}_0 - \bar{Y}), (\bar{D}_0 - \bar{Y}) \; and \; (\bar{E}_0 - \bar{Y}) . \quad (4)$$

The following values of factors were chosen: A=20%, B=20%, C=35%, D=2.75%

From the analysis of S/N ratio and the mean response characteristic, the mean values for SCRC have been predicted as shown in Table 14.

Table 14. Taguchi predicted values and actual values for SCRC.

Test	Experimental results of the confirmation mix	Taguchi predicted value	Ratio of predicted value and actual value
Slump flow	645 mm	618.28 mm	95.85 %
V-funnel	10.224 seconds	11.0663 seconds	108.31 %
Compression	19.34 MPa	20.1 MPa	96.23%
Impact	51 blows	55 blows	107.85%

A confirmation mix was performed with the selected factors (A=20%, B=20%, C=35%, D=2.75%) and the results were recorded in Table 14. These results were compared with the predicted values, illustrated in Table 14, which obtained from Minitab program. The ratio between the actual values and the predicted values are also illustrated in Table 14 which is in range of 10% difference so experimental results could be confirmed.

10. Conclusions

Taguchi Method was used to predict the mechanical properties of self-compacting rubberized concrete in terms of compressive strength and impact resistance and fresh properties in terms of slump flow diameter and V-Funnel time. The analysis shows that the proposed Taguchi technique was adequate to predict the above properties.

The study also considered examining the influence of different concrete mix proportioning parameters that included fine rubber, coarse rubber, fly ash and viscocrete contents on the studied mechanical and fresh properties.

The analysis of variance using ANOVA shows that the percentage of fine rubber replacement was the most significant parameter influencing the studied mechanical and fresh properties. The percentage contribution was 61.3%, 59.6%, 52.1% and 75.14% for slump flow diameter, V-Funnel, compressive strength and impact resistance respectively.

References

Bignozzi MC, Sandrolini F (2006). Tyre rubber waste recycling in self-compacting concrete. *Cement and Concrete Research*, 36(4), 735-739.

EFNARC (2005). The European Guidelines for self-compacting concrete: specification, production, and use. http://www.efnarc.org/ (Accessed on November 2011).

Eid FM (2003). Properties and Fields of Application of Rubberized Concrete. *M.Sc. thesis*, Menofiya University, Egypt.

Erhan G (2010). Fresh properties of self-compacting rubberized concrete incorporated with fly ash. *Materials & Structures*, 43, 1037-1048.

Ghazy MF (2012). Effect of using mortar interface and overlays in masonry behavior by using Taguchi method. *ACI Materials Journal*, title no. 109-M49.

Ghazy MF (2015). Optimization of lightweight concrete process by Gray Taguchi method. *ACI Materials Journal*, title no. 112-M34.

Khalil E, Abd-Elmohsen M, Anwar MA (2015). Impact resistance of rubberized self-compacting concrete. Construction Research Institute, National Water Research Center, Delta Barrage 13621, Egypt.

Mishra M, Panda KC (2015). Influence of Rubber on Mechanical Properties of Conventional and Self-Compacting Concrete. ITER, SOA University, Bhubaneswar 751 030, Odisha, India.

Najim KB (2012). Determination and Enhancement of Mechanical and Thermo-physical Behavior of Crumb Rubber-modified Structural Concrete. *Ph.D thesis*, The University of Nottingham.

Najim KB, Hall MR (2012). Experimental validation of plain/self-compacting rubberized concrete (PRC/ SCRC) mix designs for structural applications. *14th International Conference of Structural Faults & Repair*, 3-5 July, Edinburgh, Scotland, UK.

Najim KB, Hall MR (2012). Mechanical and dynamic properties of self-compacting crumb rubber modified concrete. *Construction and Building Materials*, 27(1), 521-530.

Ouchi M, Okamura H (1999). Self-compacting concrete: Development, present use and future. *First International RILEM Symposium on Self-compacting Concrete*, 13-15 September, Stockholm: 3-14.

Ouchi M, Okamura H (2003). Self-compacting concrete. *Journal of Advanced Concrete Technology*, 1(1), 5-15.

Taha MM, El-Dieb AS, Abd El-Wahab MA, Abdel-Hameed ME (2008). Mechanical, fracture, and microstructural investigations of rubber concrete. *Journal of Materials in Civil Engineering*, 20(10), 640-649.

Taha MR, El-Dieb A, Abd El-Wahab M (2003). Fracture toughness of concrete incorporating rubber tire particles. *International Conference on Performance of Construction Materials: A New Era of Building*, 18-20 February, Cairo, Egypt.

Zahran MA, Nasser AA (2014). Recycling of cement dust for manufacturing cement bricks. *The 7th International Conference for Development and Environment in the Arab World*, 23-25 March.

Challenge Journal of Concrete Research Letters

Review

Reinforcement corrosion in coastal and marine concrete: A review

Saha Dauji *

Bhabha Atomic Research Centre, NRB Office, Anushaktinagar, Mumbai 400094, India

ABSTRACT

Concrete is used as a structural material for construction of buildings, jetties, harbors, etc. in many coastal and marine locations. The reinforcement used in concrete is susceptible to corrosion, resulting in loss of steel area, loss of bond, expansion of the reinforcement volume leading to cracking or spalling of concrete. Marine environment induces higher corrosion of reinforcement, compared to in-land locations. Concrete exposed to tidal fluctuations, or to the action of waves and currents are among the most severely affected. Corrosion of reinforcement in concrete is of major concern in coastal and marine environment. Control and monitoring of corrosion is a big challenge to engineers. In the recent years, different investigators reported their studies in this area. Depending on the severity of the exposure conditions, different corrosion inhibitors and protection methods have been attempted with varying degrees of success. The present article presents a generic review of the corrosion issues in marine concrete. Drawing from the experiences of the various researchers, the corrosion measurements, and corrosion control schemes, including use of coated reinforcements and corrosion inhibitors are discussed. The durability performance based design of concrete in the probabilistic framework and the life cycle cost analysis for durability design decisions have been identified as the future direction of corrosion protection of coastal and marine structures.

ARTICLE INFO

Article history:
Received 25 September 2017
Revised 18 March 2018
Accepted 29 May 2018

Keywords:
Concrete
Corrosion
Marine
Reinforcement
Corrosion inhibitor

1. Introduction

Concrete is cheap, versatile and durable building material, and it is used for many structures in coastal and marine areas. Due to the humidity, temperature and saline environment, reinforcement in such concrete is prone to corrosion. Corrosion results in loss of the reinforcement area and reduction in bond stress. Additionally, under the action of waves and currents, the corrosion of reinforcement is aggravated. The corrosion products are expansive and result in cracking of concrete cover or spalling. The chemical composition of the corrosion products of reinforcement in marine concrete was investigated by Vera et al. (2009). They concluded that lepidocrocite, goethite, akaganeite and magnetite mixtures were found both in natural and simulated marine environment whereas siderite was only detected in samples exposed to a natural marine environment. In literature, different models are presented for such estimation (Guzman et al., 2011; Wang et al., 2018) considering initiation and propagation of the chloride in concrete. These estimation models are supported by laboratory and field experiments by various researchers (Kondratova et al., 2003; Pradhan, 2014; Zhu et al., 2017; Wu et al., 2017). Repairing of concrete in marine locations, especially the submerged portions, is difficult and costly. Hence, corrosion of steel in marine concrete structures has received continued attention, in attempt to prevent, monitor and control corrosion. After introduction to the topic in the present section, the present study summarizes the issues of reinforcement corrosion in marine concrete in the following section. In the subsequent sections, a review of the various schemes of corrosion monitoring and control as reported in recent literature, is presented. This is followed by concluding remarks and references. The information provided in the article

* *Corresponding author*. Tel.: +91-222-559-7985 ; E-mail address: acad.dauji@gmail.com (S. Dauji)
ISSN: 2548-0928 / DOI: https://doi.org/10.20528/cjcrl.2018.02.003

would help designers and project authorities in development of the strategies for monitoring and control of corrosion in their facilities according to the available resources, importance and service life of the concrete structures.

2. Factors Affecting Reinforcement Corrosion in Marine Concrete

Reinforcement is protected in alkaline concrete with a passive layer of corrosion products, which prevents further corrosion. This is the common situation in the concrete structures in general. To sustain this situation, some amount of moisture and oxygen would be required, and any phenomenon which upsets this balance might initiate corrosion. The peculiarity of corrosion in marine and coastal concrete lies in the physical damages which may occur to the concrete structure, and the chloride attack which is one of the main agents of corrosion of reinforcement in marine concrete. The diffusivity of the chloride in concrete, the diffusivity of sulfates in concrete, and the carbonation depth in concrete are among the major considerations. Other corrosion initiating factors may be chemical attack, salt weathering, and freeze-thaw attack among others (Neville, 1996).

2.1. Physical damages in marine concrete

The concrete may be affected by the passing currents, incident waves and splashes and sprays from breaking waves. In locations of strong wave and current action, abrasive effect of the sand, shingle and other debris in water may be significant. Surface of concrete just above ground or water level can experience salt crystallization, when salt water drawn up by capillary action evaporates, leaving behind the salt crystals – which can cause expansion damage. This problem is more pronounced in tropical climates. Horizontal slabs, when subjected to seawater spray, would be coated with salts, which move into concrete, a phenomenon known as salt scaling. The effect of these physical damages is detrimental to the durability as the cover to reinforcement is reduced, porosity of concrete is increased, and the chloride and other chemical ingress get enhanced. Any chemical deterioration of concrete like sulphate attack or alkali-silica reaction also have similar contribution to reinforcement corrosion.

Damage to concrete due to shock or impact might result in cover concrete cracking and subsequent ingress of seawater or saline air into concrete (Ramesht and Tavasani, 2013). The possible causes could be lack of using shock absorber devices or inadequate concrete cover. This assumes importance particularly for concrete the dock and jetty structures and should be given special attention.

2.2. Water level

Durability of concrete is largely influenced by its position with respect to the water level, with the maximum deterioration at average water level and above. Three zones have been identified for reinforcement corrosion in concrete, the atmospheric zone, the splash zone, and the submerged zone. In atmospheric zone, the concrete is exposed to humid and saline air, but not in direct contact with seawater. The submerged zone is where the concrete surface is saturated with limited access to oxygen. In between these two extremes, concrete is exposed to alternate wetting and drying cycles, with varying availability of oxygen (Allen, 1998). This zone may be split into tidal zone, where concrete is mostly wet, and splash zone, where concrete is mostly dry. The area of splash zone towards the drier (upper) side is most vulnerable to corrosion.

2.3. Chloride ingress

Presence of chloride ions in concrete may be due to salt contamination of the aggregates, or due to surface contamination of the reinforcing bars from air or salt-contaminated ground, or when reinforcement is inundated in low-lying areas. Chloride may also be absorbed from seawater in marine conditions. The factors governing the chloride diffusion to steel from concrete are depth of cover to reinforcement, presence of cracks in concrete, absorptivity and degree of saturation of concrete. There is difference of opinion of the mechanism of chloride ingress. The processes considered are diffusion, absorption due to capillary action and suction due to hydration of cement (Allen, 1998). After initial absorption over a few years, the chloride ingress is believed to stabilize. Roy et al. (1993) studied the chloride ingress in tropical marine concrete and reported that the diffusion coefficient calculated from field data agreed well with the earlier reported laboratory and field survey results. They further reported that the chloride ingress profiles matched with those computed from the diffusion theory. Luping (2008) proposed modeling free chloride transport taking free chloride as diffusion potential and then calculating the total chloride content taking into account the non-linear chloride binding along with the practiced empirical models based on error functions. They reported good agreement between the proposed model and the measurements though more studies for the pozzolona concrete were proposed. Such studies would help to generate additional data on which the different models could be generated and refined for further application.

2.4. Carbonation

Carbonation is the process of diffusion of carbon dioxide from air into concrete and reaction in presence of water results in carbonic acid, which reacts with the hydrated cement, starting with calcium hydroxide. This occurs even in low levels of carbon dioxide as present in the rural atmosphere. Carbonation results in lowering of the pH of concrete from around 13 and when it falls below 9, the passivity of the oxidation products on the reinforcement is broken and corrosion of reinforcement is initiated (Neville, 1996). However, carbonation is less of a problem in marine concrete compared to chloride attack. Carbonation can, of course, increase the propensity

of the reinforcement in concrete to get corroded in cases where the chloride intrusion has already initiated the process of corrosion. So, it has to be considered in the overall plan of the monitoring and control of the corrosion of reinforcement of concrete in coastal and marine structures.

2.5. Resistivity

The process of corrosion requires an electrolyte between the anode and cathode on different parts of the reinforcement. Pore water with dissolved salts provide a low resistance pathway to electrical current, thus aiding corrosion. In dry concrete, which is highly resistive, corrosion is limited.

2.6. Degree of saturation, humidity and temperature

Diffusion of gases like carbon dioxide (which lowers the pH of concrete) and oxygen (which is required for oxidation) is limited in saturated concrete. Below 50% saturation, lack of electrolyte restricts corrosion. In between these limits, rapid corrosion is possible. In marine environment, concrete in the splash zone is subjected to alternate drying and wetting. During dry phase, carbonation and oxygen ingress is rapid and during wet phase, high humidity is present – this combined action aids corrosion and reinforcement corrosion rate is very high. Hussain (2011) explained the behavior of oxygen consumption rate of corroding steel reinforcement in chloride contaminated concrete under varying moisture environmental conditions, namely air dry, submerged, 95% relative humidity and alternate wetting–drying with the experimental studies. It was reported that the diffusion of oxygen is a significant factor only in the water saturated concrete and mentioned that it may be affected by the ratio of anode area and the total volume of concrete.

Alhozaimy et al. (2012) investigated the coupled environmental effects of high humidity and high temperature on chloride corrosion marine concrete structures. Laboratory controlled experimentation was carried out with 30°C, 40°C, and 50°C with 85% relative humidity. Samples with two 10 mm diameter bars, one completely and one partially embedded, with clear cover of 15 mm, were immersed in 99.99% pure sodium chloride solution. Tests carried out include half-cell corrosion potential using copper–copper sulfate reference electrode, macro-scale corrosion analysis, micro-scale corrosion analysis, and corrosion mass loss by gravimetric method. The corrosion reaction, after the breaking of passive layer, was observed to be both non-uniform and non-linear. It was also observed that there was a decrease in corrosion potential and corrosion mass loss at 50°C compared to that at 40°C. Possible reason identified was the reduction of oxygen solubility in the pore solution at high temperature and blockage of concrete pores at high relative humidity of 85%, under which another stable oxide layer may have developed. This was suggested as a potential method to passivate rebar in chloride environment.

2.7. Intense local corrosion

Some cases of severe local corrosion have been observed where a small area of reinforcing steel is exposed to seawater in submerged zone and linked to an efficient cathode above water (Allen, 1998). This condition would be dangerous in slender structures with few bars, like piles supporting jetties, which have been somehow damaged, resulting in large scale cracking and spalling.

2.8. Stray current corrosion

In certain marine structures, the additional steelwork like pipes and risers are protected from corrosion by cathodic protection and the reinforcement in concrete is left out of the system. If the reinforcement cage is not fully isolated, which is seldom the case, it might pick up stray current and corrosion would ensue in the anodic area when steel gives up its charge to the 'ground'. Hence, it is advisable to include all steel components, including complete reinforcing cage, for cathodic protection.

2.9. Use of supplementary cementitious materials

When replacing cement with other supplementary cementitious materials, special attention should be given towards the corrosion inhibition characteristics of the resulting concrete especially if it used in marine environment. Valipour et al. (2017) evaluated the durability performance of concrete specimens cast with various supplementary cementitious materials such as natural zeolite (0 - 30% cement replacement), metakaolin (0 - 15% cement replacement) and silica fume (0 - 10% cement replacement). The study investigated chloride diffusion when those specimens were exposed to tidal and splash exposures in a harsh marine environment, along with a parallel study under laboratory conditions. The authors concluded that optimum replacement level for zeolite in concrete between 10% and 20% resulted in 60% to 70% improvement in chloride penetration resistance in terms of concrete durability in aggressive environments.

3. Monitoring Reinforcement Corrosion

In addition to periodic inspection and maintenance of the structures, some innovative schemes of corrosion monitoring have been proposed by investigators in the recent years. Taking advantage of advancement of technology, acoustic emission, cost-effective sensors, and spectroscopy methods have found application in the monitoring process and they are discussed briefly in this section.

In their paper, Martinez and Andrade (2008) proposed a method of evaluating the efficiency of the cathodic protection by using linear polarization and electrochemical impedance spectroscopy (EIS). It was inferred from the results that the AC polarization resistance results can be applied for distinguishing cathod-

ically protected steel from unprotected one, as the frequency value at which the maximum in phase angle appears for the faradic process would be moved towards higher values by around one to two orders of magnitude. The efficiency of the cathodic protection or verification of passivity can be checked by the recording of Bode plots of phase angles and verifying the frequency range of the appearance of the time constant of the faradic process. Influence of the electrolyte resistance was not noticed in any experiment. The results indicate that the impedance diagrams show important and consistent changes in shape and associated parameters when the steel is protected or unprotected and would be an efficient tool to monitor corrosion in steel exposed to saline water / environment.

Duffo and Farina (2009) developed an integrated and cost-effective sensor system for corrosion monitoring of reinforced concrete structures. It consisted of sensors, which would provide online measurements of various variables like the open circuit potential of reinforcement, the corrosion current density of bars, the electrical resistivity of concrete, the availability of oxygen, the chloride ions concentration in concrete, and the temperature inside the structure. These different electrodes, embedded in concrete were integrated with a software system that acquired and analyzed the data. Additionally, the software would generate alarms, to prompt the specialist to decide applicable mitigation strategies. From the results obtained, the promise of this particular sensor in determination of the corrosion state of existing as well as new concrete structures was established.

In salt environment, after corrosion of rebar is nucleated, the expansion of corrosion products results in corrosion-induced cracks in reinforced concrete. Kawasaki et al. (2010) evaluated acoustic emission (AE) technique for identification of the onset of corrosion and the nucleation of concrete cracking with a set of cyclic wet–dry tests of concrete specimens. Reinforcement provided was a single 13 mm diameter deformed bar embedded with 20 mm clear cover. Regular AE monitoring was performed during the wetting and drying cycle of a week each. The onset of corrosion and the nucleation of concrete cracking were clearly observed as two periods of high AE activity. Kinematics of micro-cracks was identified by SiGMA (Simplified Green's functions for moment tensor analysis) analysis of AE. The findings were corroborated with Scanning Electron Micrograph study of the cross-sections of corroded bars. It was concluded that AE techniques could be efficient tool for monitoring the corrosion process in marine concrete structures.

4. Control of Reinforcement Corrosion in Marine Concrete

There appears to be no single universal solution to the problem of reinforcement corrosion in marine concrete structures. Various approaches have been reported in literature and they would be required to be used either individually or in combination for efficient control for the corrosion scenario under consideration.

4.1. Dense compact concrete

No corrosion protection scheme would work without sound, dense and compact concrete. This would require proper mix design, workmanship, and adequate curing. There have been some studies on the effect some materials have on corrosion behavior, when they are added to the concrete mix. Asrar et al. (1999) reported that blending of sulfate resistant cement with microsilica gave better corrosion performance compared to ordinary Portland cement blended with microsilica when used for marine concrete.

In their study on predicting chloride penetration in fly ash concrete under long-term exposure in a marine environment, Chalee et al. (2009) presented empirical models developed based on two, three, four, and five year investigation of concretes in a marine site. The models were generated by regression analysis of the data, applying Fick's second law of diffusion. The model variables were the water to binder ratio, fly ash content, distance from the concrete surface, and exposure time. The prediction error of the models was around 25%-30%. The model also predicted the strong effect of fly ash and water to binder ratio on reducing chloride diffusion in concrete. It was concluded that a high volume (up to 50% of binder by weight) fly ash replacement and a low water to binder ratio would yield good chloride resistance in concrete under long-term exposure in a marine environment.

In their paper, Shekarchi et al. (2009) investigated how the strength and durability properties of concrete exposed to Persian Gulf conditions, got affected when silica fume was used as supplementary cementitious material in concrete. The chloride diffusion coefficient was also determined from samples taken at the ages of three, nine and thirty-six months. From the results, it was inferred that partial cement replacement up to 7.5% with silica fume reduces the chloride diffusion coefficient, while for higher replacement up to 12.5%, decrease in the diffusion coefficient was not significant. Though there was not much improvement in final strength, the initial rate of strength development was higher in silica fume concrete compared to ordinary Portland cement concrete. It was suggested that a silica fume content of 7.5–10% by weight of cement would be optimum for preventing chloride ingress in marine concrete for corrosion protection.

Chalee et al. (2010) investigated the effect of fly ash replacement in concrete and concluded that that the increase in fly ash clearly reduced the chloride penetration, chloride penetration coefficient, and steel corrosion in concrete. They presented an empirical model which could predict the concrete cover required to protect against corrosion initiation, within +15% of their experimental data and +25% of the last 10 years' data reported by other researchers for marine concrete.

In their study Lopez-Calvo et al. (2012) investigated the effect of calcium nitrite based corrosion inhibitor (CNI) and fly ash (FA) on the long-term compressive strength of high performance concrete (HPC). For twenty-eight day and one year strength, cylinders were tested while for nine year strength, concrete cubes were

obtained from reinforced concrete slabs that had been exposed to a marine environment. It was observed that there was an enhancement on the compressive strength in concrete even after long-term exposure to a marine environment.

4.2. Cracking and cover to reinforcement

Cracks inevitably form on the concrete surface due to plastic shrinkage, drying shrinkage and thermal contraction. Possible remedies include low water-binder ratio, using low heat cement and supplementary cementitious materials of low heat of hydration, proper and adequate curing, lowering placement temperature and limit the temperature differential to around 20°C.

The importance of adequate cover to concrete in control of corrosion cannot be overemphasized. The cover provides a space to place and compact concrete where it is vital from durability point of view. The cover provides the minimum reservoir of alkalinity around reinforcement, and helps to maintain its passivity. Furthermore, cover acts as a barrier against chloride ingress and carbonation. For a certain crack width at surface of concrete, the crack width at the bar surface decreases with increasing cover depth, thus limiting chloride penetration, carbonation and corrosion.

4.3. Concrete surface treatments

There have been several studies on the corrosion protection by treating the surface of concrete with some coating material or mortar. The desirable properties of concrete surface coatings would include water impermeability, water vapor permeability, thermal stability, adequate adhesion, crack-bridging ability, and adequate elasticity.

Spainhour and Wootton (2008) investigated the performance of steel reinforcement embedded in concrete samples, encased by carbon fiber reinforced polymer (CFRP) wraps. Concrete samples were wrapped with 0 to 3 fabric layers impregnated with two different epoxies. Corrosion was accelerated by an impressed current through the samples kept in a high salinity solution. Corrosion was monitored dynamically during exposure by current flow measurements and reinforcement mass losses were measured after exposure. When comparing the theoretical predictions of total mass loss with actual corrosion mass loss values from experiment, it was found that in general the calculated mass loss under-predicts the actual amount of corrosion mass loss, though these two were well correlated. Test results indicated that CFRP wrapped specimens had decreased reinforcement mass loss, and lowered the corrosion rates. The performance of wrapped specimens was found superior to that of either control samples or those coated only with epoxy. Results indicated that in saline environment, the corrosion protection provided by the CFRP wraps improved with the more suitability of epoxy used, and the number of CFRP wrap layers.

Medeiros and Helene (2009) studied the efficacy of some surface treatments like hydrophobic agents, acrylic coating, polyurethane coating, and double systems in inhibiting chloride penetration in concrete. The efficiency of the coating was evaluated with tests like capillary water absorption test, pipette absorption test, chloride diffusion coefficient in saturated concrete, and rapid chloride penetration test. It was observed that the double systems presented greater capacity for reducing the capillary water absorption and chloride diffusion than all the single protection systems, with polyurethane coating as an exception. It was also noticed that all the tested surface protection coating provided significant reduction (>70%) in the sorptivity of concrete. In their effectiveness in reducing the chloride diffusion coefficient, polyurethane coating was the best with a reduction rate of 86%, followed by the double systems with best reduction of about 40%, and best reduction of other single coatings was around 20%. It was concluded that among the studied surface treatments, the polyurethane coating was the best corrosion protection surface treatment for marine concrete.

In their paper, Dai et al. (2010) examined the effectiveness of a water reducer and chloride barrier surface impregnation of the reinforced concrete in a marine environment with focus on how surface cracks created before and after impregnation influenced their performance. Reinforced concrete prisms and cylinders, treated with silane-based water repellent agents and sodium silicate-based pore blockers, were exposed to cyclic sea water shower under an outdoor environment for one year. Under such simulated accelerated subtropical marine wet-dry cycles, the time-dependent water absorption of all specimens was monitored. The penetration depths of the surface impregnation agents and the chloride penetration profiles were determined by splitting the samples. The areas with corrosion, evident in the steel reinforcement of the specimens were also measured.

From the results, it was observed that the sodium silicate-based pore blockers were not effective in preventing chloride penetration into concrete under simulated marine conditions. Under similar conditions, silane-based impregnation was found to be a highly effective in reducing water and chloride absorption, and the efficiency depended on the penetration depth, larger than 5 mm being advocated. When cracks (up to 0.2 mm) existed before impregnation, impregnation with silane-based cream and gel could resist corrosion even after one year of accelerated dry/wet exposure to salt water. However, if cracks formed after impregnation, chloride penetration could not be totally prevented, other than very fine cracks (< 0.08 mm).

Zhang et al. (2010a) explored geopolymer as an innovative inorganic coating for corrosion protection in marine concrete. The properties examined were setting time, permeability, anticorrosion, bond strength, and volume stability. A compound geopolymer was developed by adding 10% granulated blast furnace slag (GBFS) in metakaolin, and a beneficial effect of GBFS was observed in reducing the permeability of the geopolymer. From the study, it was confirmed that geopolymer had excellent anticorrosion property in seawater as well as marine atmosphere. Possibly due to the coexistence of calcium silicate hydrate (C–S–H) gels in both cement and

geopolymer matrix, the average bond strength between geopolymer and cement paste or between geopolymer and mortar was found to be higher than 1.5 MPa. The large shrinkage of the geopolymer could be controlled with addition of polypropylene (PP) fiber and MgO expansion agent, and careful early age curing. It was inferred that geopolymer can be applied as an innovative protective coating for marine concrete structures.

The earlier study was followed by an investigation by Zhang et al. (2010b) on the microstructure of the interfaces between the geopolymer and cement paste and mortar, and the pore structure of geopolymers. The various tools applied included scanning electron microscopy (SEM), mercury intrusion porosimetry (MIP) and Brunauer–Emmett–Teller (BET) nitrogen adsorption. It was found that the interface between the geopolymer and cement paste was very compact and its chemical composition changed due to the reaction between the geopolymer slurry and the cement. Open pores in the geopolymer were much smaller than that of ordinary Portland cement paste. The permeability decreased due to the compact microstructure of the geopolymer. The alumino-silicate geopolymerization products, unlike the hydration products of ordinary Portland cement, were stable both under sea water and in marine atmosphere, thus retaining their protective properties. It was suggested from the analysis that metakaolin-based geopolymers could be used as corrosion protection for marine concrete structures.

In their paper, Moradllo et al. (2012) explored six different concrete surface coatings, namely, acrylic modified cementitious coating, epoxy polyurethane, aliphatic acrylic (solvent based) with low viscosity silane/siloxane primer, acrylic modified cementitious coating, cementitious coating, styrene acrylate (solvent based) with low viscosity silane/siloxane primer on the surface of concrete and monitored their performance during 5 years of exposure in tidal zone of Persian Gulf region. Tidal exposure was at about 2.2 m from sea level, where the durations of exposure of concrete to dry and wet conditions were similar, like the tidal zone. The tests included chloride profile, chloride diffusion coefficient, surface chloride content, time dependent surface chloride content, and surface coating lifetime study. From the results, it was inferred that epoxy polyurethane and aliphatic acrylic were the most efficient coatings, which cause a reduction the chloride penetration and enhance the service life of concrete structures. However, performance of surface coatings is time-dependent and deterioration with time was observed.

Gong et al. (2012) evaluated the corrosion performance of marine concrete, with surface treatment by silane impregnation, using silane gel and silane solution. Effect of the type and amount of silane on the mechanical performance, capillary water absorption and chloride ion permeability of concrete were studied in the experiments. It was observed that, compared to untreated concrete, there was around 90% reduction of water absorption and chloride absorption of treated concrete. The chloride diffusion coefficient and electric flux was also found to decrease considerably. The reduction achieved was more in silane gel than silane solution treatment, and it also increased with amount of silane applied. It was inferred that surface treatment of concrete with silane was an effective chloride corrosion inhibitor in marine conditions.

Al-Majidi et al. (2018) presented a novel method of corrosion affected concrete repair using waste material rather than primary mineral product. They used strain hardening fibre reinforced geopolymer concrete for coating concrete which was subjected to accelerated corrosion and subsequent flexural tests of beam specimens. They concluded that surface coating with polyvinyl alcohol fibre reinforced geopolymer concrete significantly reduced corrosion damage in terms of mass loss, crack distributions and structural performance. A further observation was that the differences in surface coating thickness considerably affected the corrosion resistance of the repaired beams.

4.4. Coated reinforcement

Venkatesan et al. (2006) examined the performance of three different types of corrosion protection by specialty coatings to reinforcement bars, namely cement polymer composite (CPCC), interpenetrating polymer network coating (IP) and epoxy coating as corrosion inhibitors for marine concrete. They concluded that over the one year study period, the CPCC performed best for atmospheric, high tide and sea floor level, whereas epoxy performed better than IP for high tide level and the sea floor level.

The corrosion performance of epoxy/zinc duplex coated 13 mm diameter reinforcement, embedded in concrete was compared by Dong et al. (2012) with the black steel, galvanized and epoxy coated ones. The mechanical damages of epoxy coatings, which might occur during placement and casting of concrete, affect the corrosion protection performance and this aspect was also examined. The bars were placed with a cover of 12 mm, at the center of concrete cylinders, and immersion/exposure experiment was carried out on an ocean test platform, in the strait across Xiamen and Gulangyu, China. The specimens were subjected to two simulated accelerated tidal cycles per day. The corrosion potential of rebar embedded inside concrete specimens was measured by a digital multimeter with reference to saturated calomel electrode. The epoxy coated and epoxy/zinc duplex coated bars showed better anti-corrosion performance than others. While considering the mechanical damage of about 0.928% of the total surface area of coated rebar, more severe corrosion was observed in the damaged area of epoxy coated bar. In contrast, the epoxy/zinc duplex coating remained a good corrosion protection to steel in concrete even when suffering from similar mechanical damages to the epoxy coats.

Shubina et al. (2016) explored a new generation of reinforcement coatings for corrosion resistance. This was bio-molecules which was an eco-friendly option of reinforcement coating. The evaluation of the effectiveness of this coating was performed in simulated concrete pore solution using classical electrochemical measurements, microscope observations and X-ray Photoelectron Spectroscopy (XPS). They concluded that bio-molecules with

the concentration of 1 g L^{-1} were demonstrated inhibition efficiency against corrosion of carbon steel in simulated concrete pore solution. For actual application, further investigation of inhibition properties of bio-molecules in the real mortar-embedded reinforcement bars along with evaluation of impact on the ecosystems would be required before the full-scale applications biomolecules.

4.5. Other reinforcement

There have been attempts at using other materials like stainless steel, galvanized reinforcement, and fibers as reinforcement in concrete in different research initiatives. However, due to some limitations, these have not been practically implemented. Stainless steel is prohibitively costly, and there are problems in large scale production of mild steel clad in stainless steel for corrosion protection. From their probabilistic life cycle analysis, Val and Stewart (2003) concluded that use of stainless steel reinforcement, which was six to nine times more expensive than carbon steel reinforcement, would be justified if the construction cost using stainless steel was no more than about 14% higher than the construction cost of using carbon steel reinforcement, for the splash zone. Galvanization of reinforcement may react with the alkaline concrete to give off hydrogen gas, which would pose fresh problems. Furthermore, research indicates that at high chloride levels, galvanization does not offer much benefit. Mild steel, stainless steel and polypropylene fibers have been used. Though they offer many benefits like strength equal to or greater than reinforcing bars, reduced weight and enhanced durability, their practical application have been limited to the armoring layers for abrasion protection of structural concrete. Further, they have found wide-spread application in the repair and rehabilitation of distressed concrete structures.

4.6. Cathodic protection

Prevention of corrosion of reinforcing steel has also been tried with cathodic protection devices, where sacrificial anodes are used. Bertolini et al. (2002) conducted experiments on reinforced concrete columns with steel embedded in chloride free and chloride contaminated concrete. They concluded that the sacrificial anodes were very effective in prevention of the initiation of the corrosion, and comparatively less effective in controlling any already initiated pitting corrosion. Orlikowski et al. (2004) established from their experiments that the proposed mix of pigmentary graphite and polymer matrix were very effective in cathodic protection of the reinforcement in concrete provided the graphite content was kept between 40% and 45%. Bertolini et al. (2004) reported the behavior of anode made of nickel-coated carbon fibres in a cementitious mortar used as cathodic protection. They further attempted patch repair on anode areas damaged by excessive current and concluded that such repairs were not effective.

A paper by Bertolini and Redaelli (2009) dealt with the determination of current and potential distribution in reinforced concrete elements partially submerged in seawater. The study was aimed at predicting the throwing power of cathodic prevention applied by means of sacrificial anodes. Throwing power means the height at which protection can be achieved with the particular anode location. It had been earlier reported that for cathodic protection, this height was limited to a few tens of centimeters above the water level, depending on the concrete resistivity. It was suggested that due to the higher polarisability of passive steel compared to that of active steel, the use of cathodic prevention, could be one option to overcome the limitation of cathodic protection. Experimental results from previous laboratory tests showed that the throwing power of cathodic prevention is higher compared to that of cathodic protection. Numerical simulations with finite element models of potential distribution were carried out for extending the results obtained on small-scale specimens to elements of larger dimensions, for both cathodic protection and cathodic prevention. The electrochemical behavior of steel bars, geometry of the pile, geometry of sacrificial anodes, concrete resistivity and water level were varied in the study. It was concluded that the throwing power of protection was influenced by the geometry of the pile, in particular its diameter, and by the amount of steel surface to be protected while other parameters such as concrete cover, position and dimension of submerged anodes showed no effects in the ranges of variation considered. Submerged sacrificial anode could inhibit corrosion up to 1.2 m above the water level.

Xu and Yao (2011) proposed a conductive overlay material made of carbon fiber filled cementitious mortar for cathodic protection of reinforced concrete structures. The main advantages of this scheme over the other anodic materials were noted as the similarity of thermal expansion to that of the underlying concrete and low contact resistance between the anode material and the concrete. Although there would be increase in cost by adopting this material and processing procedure, it would be compensated by the ease of installation, especially in inaccessible locations. The mechanical, electrical, and electrochemical properties of the material were investigated to evaluate the practicability. It was reported that the addition of carbon fibers enhanced the strength and toughness of the mortar, as well as the electrical performance. It was suggested that the optimum fiber content should be above but in the vicinity of the percolation threshold. It was ascertained from the accelerated anodic polarization tests and impedance measurements that both of the fiber content and pore solution composition influence the electrochemical property. The work confirmed the possible utilization of this type of anode material in cathodic protection of reinforced concrete damaged by chloride induced corrosion as in marine environment.

5. Life Cycle Analysis, Probabilistic and Durability Based Approaches

Zen (2005) discussed life cycle management for steel piles in sea water. Similar approach would be required to be adopted for efficient corrosion management of

reinforced concrete structures too. In this regard, Meira et al. (2010) reported that the results of numerical extrapolations from their experimental data showed that chloride deposition rate on the wet candle can be used as an environmental indicator, helping to estimate the expectancy of service life of concrete structures or suggesting minimum concrete cover thicknesses for a required service life. Porsaee (2009) presented a measurement unit and a flexible program to facilitate the automated measurements of corrosion activity of reinforcement bars embedded in concrete, using a variety of electrochemical techniques. Such approaches must be further customized for application in corrosion monitoring of the coastal and marine concrete structures.

Val and Stewart (2003) presented the results of the probabilistic life-cycle cost analysis which could be applied to select optimal strategies for improvement of durability of reinforced concrete structures in marine environments considering the serviceability criteria like spalling and cracking. A probabilistic approach to durability was proposed for the design of reinforced cover of a concrete immersed in sea water by Deby et al. (2009). It considered non-linear chloride diffusion model, probabilistic parameter variability, and cement chemical composition, among others. The model was developed for ordinary Portland cement. Similar studies for other types of cement, and admixtures would be very useful. A design approach based on the verification of the serviceability (durability) limit states, such as de-passivation of reinforcement, cracking and spalling due to corrosion, and collapse due to cross section loss of reinforcement was advocated for marine environment by Ferreira (2010) based on the probability based durability performance analysis. The potential of the approach for assisting in durability design decision making process was highlighted.

When evaluating the possibility of corrosion in marine concrete or planning mitigation strategies, all possible causes and factors need to be considered. De Medeiros-Junior et al. (2015) demonstrated the practical approach with a case study of corrosion in an offshore platform. They concluded that the progression of corrosion depended on the orientation of the analyzed structure (sidewalls, towards wind / wave action or away) and this should be considered in studies of expected service life to be employed in real situations. They further mentioned the commonly found pathological manifestations in the structure under study as cracks, concrete detachment, marine growth and concrete displacing by reinforcement corrosion.

6. Conclusions

The major issues regarding reinforcement corrosion in marine and coastal concrete structures have been briefly discussed. The chloride attack is the main process governing corrosion with concrete in the splash zone being the most vulnerable. Higher humidity and higher temperature aid the process of corrosion. Physical damages by sand, shingles and debris carried by waves and currents as well as impact from vessels aggravate the problem. When cathodic protection is provided to additional steelwork, the reinforcement should also be cathodically protected to avoid stray current corrosion.

The main strategy for monitoring corrosion would be periodic and methodical inspection and maintenance. Other promising options like installation of sensors and advanced techniques like acoustic emission and spectroscopy have been identified by researchers and may be implemented as and when required. Automated measurement of the corrosion performance of reinforcement in marine concrete had been suggested. Dense and compact concrete, produced with low heat cement / cementitious material, low water-binder ratio, placed and compacted properly, and cured adequately would be indispensable in providing protection against corrosion. Depending upon the atmospheric aggression, adequate cover thickness should be provided. Use of stainless steel or galvanized steel as reinforcement has found limited practical application. The fiber reinforced concrete has been utilized, in majority of cases, as abrasion resisting armor for structural concrete. Epoxy-coated reinforcement and duplex coated reinforcements have also been proposed.

Majority of the work in the recent years have concentrated on various surface treatments of concrete like carbon fiber reinforced polymer, geopolymer, silane based coatings, among others. Some experiments have also been performed on cathodic protection schemes. It must be noted that there does not exist a single solution to the problem of reinforcement corrosion and systematic evaluation of the case under consideration should be performed to arrive at the most effective measure to prevent and limit corrosion of reinforcement in marine and coastal concrete structures. Keeping in view the variety of factors involved in the durability performance of marine concrete, and their complex non-linear interactions, probabilistic models had been proposed for predicting the performance. Further, performance based design and life cycle cost analysis which incorporates the stochastic nature of the variables would be essential in improving the design as well as the performance of the concrete structures in coastal and marine locations.

References

Alhozaimy A, Hussain RR, Al-Zaid R, Al-Negheimish (2012). A Coupled effect of ambient high relative humidity and varying temperature marine environment on corrosion of reinforced concrete. *Construction and Building Materials,* 28, 670–679.

Allen RTL (1998). Concrete in Coastal Structures. Thomas Telford Publishing, London, UK.

Al-Majidi MH, Lampropoulos AP, Cundy AB, Tsioulou OT, Al-Rekabi S (2018). A novel corrosion resistant repair technique for existing reinforced concrete (RC) elements using polyvinyl alcohol fibre reinforced geopolymer concrete (PVAFRGC). Construction and Building Materials, 164, 603–619.

Asrar N, Malik AU, Ahmad S, Mujahid FS (1999). Corrosion protection performance of microsilica added concretes in NaCl and seawater environments. *Construction and Building Materials,* 13, 213-219.

Bertolini L, Bolzoni F, Pastore T, Pedeferri P (2004). Effectiveness of a conductive cementitious mortar anode for cathodic protection of steel in concrete. *Cement and Concrete Research*, 34, 681–694.

Bertolini L, Gastaldi M, Pedeferri MP, Redaelli E (2002). Prevention of steel corrosion in concrete exposed to seawater with submerged sacrificial anodes. *Corrosion Science,* 44, 1497–1513.

Bertolini L, Redaelli E (2009). Throwing power of cathodic prevention applied by means of sacrificial anodes to partially submerged marine reinforced concrete piles: Results of numerical simulations. *Corrosion Science,* 51, 2218–2230.

Chalee W, Ausapanit P, Jaturapitakkul C (2010). Utilization of fly ash concrete in marine environment for long term design life analysis. *Materials and Design,* 31, 1242–1249.

Chalee W, Jaturapitakkul C, Chindaprasirt P (2009). Predicting the chloride penetration of fly ash concrete in seawater. *Marine Structures,* 22, 341–353.

Dai JG, Akira Y, Wittmann FH, Yokota H, Zhang P (2010). Water repellent surface impregnation for extension of service life of reinforced concrete structures in marine environments: The role of cracks. *Cement & Concrete Composites,* 32, 101–109.

Deby F, Carcassès M, Sellier A (2009). Probabilistic approach for durability design of reinforced concrete in marine environment. *Cement and Concrete Research,* 39, 466–471.

De Medeiros-Junior RA, De Lima MG, De Brito PC, De Medeiros MHF (2015). Chloride penetration into concrete in an offshore platform - analysis of exposure conditions. Ocean Engineering, 103, 78–87.

Dong SG, Zhao B, Lin CJ, Du RG, Hu RG, Zhang GX (2012). Corrosion behavior of epoxy/zinc duplex coated rebar embedded in concrete in ocean environment. *Construction and Building Materials,* 28, 72–78.

Duffó GS, Farina SB (2009). Development of an embeddable sensor to monitor the corrosion process of new and existing reinforced concrete structures. *Construction and Building Materials,* 23, 2746–2751.

Ferreira RM (2010). Optimization of RC structure performance in marine environment, *Engineering Structures,* 32, 1489-1494.

Gong C, Jianzhong L, Cuicui C, Changfeng L, Liang S (2012). Study on silane impregnation for protection of high performance concrete. *Chinese Materials Conference, Procedia Engineering,* 27, 301–307.

Guzmán S, Gálvez JC, Sancho JM (2011). Cover cracking of reinforced concrete due to rebar corrosion induced by chloride penetration. *Cement and Concrete Research,* 41, 893–902.

Hussain RR (2011). Effect of moisture variation on oxygen consumption rate of corroding steel in chloride contaminated concrete. *Cement & Concrete Composites,* 33, 154–161.

Kawasaki Y, Tomoda Y, Ohtsu M (2010). AE monitoring of corrosion process in cyclic wet–dry test. *Construction and Building Materials,* 24, 2353–2357.

Kondratova IL, Montes P, Bremner TW (2003). Natural marine exposure results for reinforced concrete slabs with corrosion inhibitors. *Cement & Concrete Composites,* 25, 483–490.

Lopez-Calvo HZ, Montes-Garcia P, Bremner TW, Thomas MDA, Jiménez-Quero VG (2012). Compressive strength of HPC containing CNI and fly ash after long-term exposure to a marine environment. *Cement & Concrete Composites,* 34, 110–118.

Luping T (2008). Engineering expression of the ClinConc model for prediction of free and total chloride ingress in submerged marine concrete. *Cement and Concrete Research,* 38, 1092–1097.

Martínez I, Andrade C (2008). Application of EIS to cathodically protected steel: Tests in sodium chloride solution and in chloride contaminated concrete. *Corrosion Science,* 50, 2948–2958.

Medeiros MHF, Helene P (2009). Surface treatment of reinforced concrete in marine environment: Influence on chloride diffusion coefficient and capillary water absorption. *Construction and Building Materials,* 23, 1476–1484.

Meira GR, Andrade C, Alonso C, Borba Jr. JC, Padilha Jr. M (2010). Durability of concrete structures in marine atmosphere zones – The use of chloride deposition rate on the wet candle as an environmental indicator. *Cement & Concrete Composites,* 32, 427–435.

Moradllo MK, Shekarchi M, Hoseini M (2012). Time-dependent performance of concrete surface coatings in tidal zone of marine environment. *Construction and Building Materials,* 30, 198–205.

Neville AM (1996). Properties of Concrete. Fourth Edition, Addison Wesley Longman, Essex, England.

Orlikowski J, Cebulski S, Darowicki K (2004). Electrochemical investigations of conductive coatings applied as anodes in cathodic protection of reinforced concrete. *Cement & Concrete Composites,* 26, 721–728.

Poursaee A (2009). Automatic system for monitoring corrosion of steel in concrete. *Advances in Engineering Software,* 40, 1179–1182.

Pradhan B (2014). Corrosion behavior of steel reinforcement in concrete exposed to composite chloride–sulfate environment. Construction and Building Materials, 72, 398–410.

Ramesht MH, Tavasani MAM (2013). A Case Study on Corrosion in Concrete Floating Docks in Qeshm Port. *Procedia Engineering*, 54, 109–116.

Roy SK, Chye LK, Northwood DO (1993). Chloride ingress in concrete as measured by field exposure tests in the atmospheric, tidal, and submerged zones of a tropical marine environment. *Cement and Concrete Research*, 23, 1289–1306.

Shekarchi M, Rafiee A, Layssi H (2009). Long-term chloride diffusion in silica fume concrete in harsh marine climates. *Cement & Concrete Composites,* 31, 769–775.

Shubina V, Gaillet L, Chaussadent T, Meylheuc T, Creus J (2016). Biomolecules as a sustainable protection against corrosion of reinforced carbon steel in concrete. Journal of Cleaner Production, 112, 666–671.

Spainhour LK, Wootton IA (2008). Corrosion process and abatement in reinforced concrete wrapped by fiber reinforced polymer. *Cement & Concrete Composites,* 30, 535–543.

Val DV, Stewart MG (2003) Life-cycle cost analysis of reinforced concrete structures in marine environments. *Structural Safety,* 25, 343–362.

Valipour M, Shekarchi M, Arezoumandi M (2017). Chlorine diffusion resistivity of sustainable green concrete in harsh marine environments. Journal of Cleaner Production, 142, 4092–4100.

Venkatesan P, Palaniswamy N, Rajagopal K (2006). Corrosion performance of coated reinforcing bars embedded in concrete and exposed to natural marine environment. *Progress in Organic Coatings,* 56, 8–12.

Vera R., Villarroel M, Carvajal AM, Vera E, Ortiz C (2009). Corrosion products of reinforcement in concrete in marine and industrial environments. *Materials Chemistry and Physics,* 114, 467–474.

Wang Y, Wu L, Wang Y, Li Q, Xiao Z (2018). Prediction model of long-term chloride diffusion into plain concrete considering the effect of the heterogeneity of materials exposed to marine tidal zone. *Construction and Building Materials*, 159, 297–315.

Wu L, Li W, Yu X (2017). Time-dependent chloride penetration in concrete in marine Environments. *Construction and Building Materials*, 152, 406–413.

Xu J, Yao W (2011). Electrochemical studies on the performance of conductive overlay material in cathodic protection of reinforced concrete. *Construction and Building Materials,* 25, 2655–2662.

Zen K (2005). Corrosion and life cycle management of port structures. *Corrosion Science,* 47, 2353–2360.

Zhang Z, Yao X, Zhu H (2010a). Potential application of geopolymers as protection coatings for marine concrete I. Basic properties. *Applied Clay Science,* 49, 1–6.

Zhang Z, Yao X, Zhu H (2010b). Potential application of geopolymers as protection coatings for marine concrete II. Microstructure and anticorrosion mechanism. *Applied Clay Science*, 49, 7–12.

Zhu W, Francois R, Liu Y (2017). Propagation of corrosion and corrosion patterns of bars embedded in RC beams stored in chloride environment for various periods. *Construction and Building Materials*, 145, 147–156.